Check for updates

Appressorium-mediated plant infection by *Magnaporthe oryzae* is regulated by a Pmk1-dependent hierarchical transcriptional network

Míriam Osés-Ruiz [1]✉, Neftaly Cruz-Mireles[1,7], Magdalena Martin-Urdiroz[2,7], Darren M. Soanes [2], Alice Bisola Eseola[1], Bozeng Tang[1], Paul Derbyshire[1], Mathias Nielsen [3], Jitender Cheema[3], Vincent Were[1], Iris Eisermann[1], Michael J. Kershaw[2], Xia Yan [1], Guadalupe Valdovinos-Ponce [4,5], Camilla Molinari [1], George R. Littlejohn [2,6], Barbara Valent [4], Frank L. H. Menke [1] and Nicholas J. Talbot [1]✉

Rice blast is a devastating disease caused by the fungal pathogen *Magnaporthe oryzae* that threatens rice production around the world. The fungus produces a specialized infection cell, called the appressorium, that enables penetration through the plant cell wall in response to surface signals from the rice leaf. The underlying biology of plant infection, including the regulation of appressorium formation, is not completely understood. Here we report the identification of a network of temporally coregulated transcription factors that act downstream of the Pmk1 mitogen-activated protein kinase pathway to regulate gene expression during appressorium-mediated plant infection. We show that this tiered regulatory mechanism involves Pmk1-dependent phosphorylation of the Hox7 homeobox transcription factor, which regulates genes associated with induction of major physiological changes required for appressorium development—including cell-cycle control, autophagic cell death, turgor generation and melanin biosynthesis—as well as controlling a additional set of virulence-associated transcription factor–encoding genes. Pmk1-dependent phosphorylation of Mst12 then regulates gene functions involved in septin-dependent cytoskeletal re-organization, polarized exocytosis and effector gene expression, which are necessary for plant tissue invasion. Identification of this regulatory cascade provides new potential targets for disease intervention.

Rice blast disease is an important threat to global food security[1]. The disease starts when asexual spores of *Magnaporthe oryzae*, called conidia, land on the hydrophobic surface of a rice leaf inducing differentiation of an infection cell called an appressorium[1–3]. The appressorium develops turgor of up to 8.0 MPa due to glycerol accumulation, which generates osmotic pressure[4]. Glycerol is maintained in the appressorium by melanin in the cell wall, which reduces its porosity[4,5]. Development of the appressorium is tightly linked to the cell cycle, autophagy[6–8] and metabolic checkpoint control mediated by TOR kinase and the cAMP-dependent protein kinase A (PKA) pathway[9–11]. Appressorium turgor is monitored by a sensor kinase, Sln1, and once a threshold is reached[12], septin GTPases in the appressorium pore form a hetero-oligomeric complex that scaffolds cortical F-actin at the base of the appressorium[13,14]. This leads to force generation to pierce the cuticle with a rigid penetration hypha. Once inside the leaf, invasive hyphae colonize the first epidermal cell before seeking out plasmodesmata-rich pit fields through which the fungus invades neighbouring cells[15]. *M. oryzae* actively suppresses plant immunity using fungal effector proteins delivered into plant cells[16]. After five days, disease lesions appear from which the fungus sporulates to colonize neighbouring plants.

Formation of an appressorium by *M. oryzae* requires a conserved pathogenicity mitogen-activated protein kinase (MAPK), called Pmk1 (ref. [17]). Pmk1 mutants cannot form appressoria or cause plant infection, even when plants are wounded[17]. Instead, Δ*pmk1* mutants produce undifferentiated germlings that undergo several rounds of mitosis and septation[17,18]. Pmk1 is also responsible for lipid and glycogen mobilization to the appressorium, autophagy in the conidium[4,8,19,20] and invasive cell-to-cell movement[15]. A set of pl surface sensors[21] that trigger cAMP–PKA signalling are required for Pmk1 activation[17], and a TOR-dependent nutrient sensing pathway is necessary for appressorium formation, acting upstream, or perhaps independently, of Pmk1 (refs. [9–11]). The mechanism by which Pmk1 exerts such an important role in plant infection has remained largely unknown and only one transcriptional regulator, Mst12, which may act downstream of Pmk1, has been characterized in detail. Mst12 mutants form appressoria normally but are non-functional and cannot cause disease[22].

In this study we set out to identify the mechanism by which major transcriptional changes are regulated during appressorium development by *M. oryzae*. We identified major temporal changes in gene expression in response to an appressorium-inductive hydrophobic

[1]The Sainsbury Laboratory, Norwich Research Park, University of East Anglia, Norwich, UK. [2]School of Biosciences, University of Exeter, Exeter, UK. [3]John Innes Centre, Norwich Research Park, Norwich, UK. [4]Department of Plant Pathology, Kansas State University, Manhattan, KS, USA. [5]Present address: Department of Plant Pathology, Colegio de Postgraduados, Montecillo, Texcoco, Mexico. [6]Present address: Department of Biological and Marine Sciences, University of Plymouth, Drakes Circus, Plymouth, UK. [7]These authors contributed equally: Neftaly Cruz-Mireles and Magdalena Martin-Urdiroz. ✉e-mail: miriam.oses-ruiz@tsl.ac.uk; nick.talbot@tsl.ac.uk

surface, which require Pmk1 or Mst12. We provide evidence that a hierarchical network of transcription factors (TFs), regulated by the Pmk1 MAPK, are necessary for the complex transcriptome changes associated with appressorium-mediated plant infection.

Results

The Pmk1 MAPK is necessary for appressorium development in response to surface hydrophobicity. *M. oryzae* develops appressoria when spores are incubated in water on hard hydrophobic surfaces. They form within 6 h and septins accumulate at the base of the incipient appressorium in a ring structure by 8 h (ref. [13]; Extended Data Fig. 1a). A single round of mitosis occurs and the conidium undergoes autophagy and degradation of its three nuclei[8], resulting in a single appressorium nucleus by 14 h (Extended Data Fig. 1a). By contrast, when *M. oryzae* conidia germinate on a hydrophilic surface, they do not undergo autophagy and develop undifferentiated germlings[11] (Extended Data Fig. 1a,b)[6]. Multiple rounds of mitosis occur and by 24 h approximately 50% of germlings contain >4 nuclei (Extended Data Fig. 1a,b). Similarly, Pmk1 mutants do not undergo autophagy or develop appressoria and instead form undifferentiated germlings (Fig. 1a and Extended Data Fig. 1c,d)[17,20]. The response of the fungus to a hydrophilic surface[10] therefore mirrors that of Pmk1 mutants.

We first determined the global transcriptional response of *M. oryzae* to surface hydrophobicity compared with that associated with loss of Pmk1. We isolated total RNA from a wild-type strain of *M. oryzae*, Guy11, at different time points during appressorium development on hydrophobic glass coverslips (hereafter referred to as HP) and hydrophilic Gelbond membranes (hereafter called HL), from 0–24 h after inoculation. In parallel, we incubated conidia of a Δ*pmk1* mutant on an HP surface for an identical time period and carried out RNA sequencing analysis (RNA-seq). Differentially expressed genes (DEGs) were defined using a *P* value adjusted for the false-discovery rate ($P_{adj} < 0.01$) and a moderated log$_2$-transformed fold change in gene expression (mod_lfc) > 1 to define upregulated genes and mod_lfc < −1 to define downregulated genes (Fig. 1b,c). We observed 3,917 *M. oryzae* DEGs in response to surface hydrophobicity (HP versus HL) and 6,333 DEGs in a Δ*pmk1* mutant compared with the isogenic wild-type Guy11 (Supplementary Tables 1 and 2). A comparison of these gene sets identified 3,555 DEGs in response to an HP surface and the presence of Pmk1, a small set of 362 Pmk1-independent DEGs in response to HP surfaces and 2,778 Pmk1-dependent genes not showing differential expression (Fig. 1d and Supplementary Table 3). We conclude that 90% of the DEGs in *M. oryzae* in response to surface hydrophobicity are Pmk1-dependent.

The set of 3,555 HP- and Pmk1-dependent genes identified functions associated with appressorium morphogenesis, such as autophagy[6,8]. Seven *ATG* genes, for example, were highly expressed during the early stages of appressorium development and downregulated from 8 h onwards (Supplementary Fig. 1). Similarly, cell cycle-related genes were differentially regulated in response to HP surfaces[23] and many were Pmk1-dependent (Supplementary Fig. 2). Genes encoding cyclins, the cyclin-dependent kinase *CDC28* and its positive and negative regulators *MIH1* and *SWE1*, respectively[24], all showed expression peaks at 4–6 h, coincident with appressorium morphogenesis (Supplementary Figs. 2 and 3). By contrast, cyclin-associated gene expression was delayed and CDK-related gene expression oscillated abnormally in the Δ*pmk1* mutants. Genes required for the DNA damage response pathway[25], such as *DUN1*, were mis-regulated in the Δ*pmk1* mutants. Fifty of the 79 known G protein-coupled receptors in *M. oryzae*[26] were differentially regulated in response to HP and 48 were Pmk1-dependent (Supplementary Fig. 4). Analysis of the DEGs additionally implicated 14 acetyltransferases, 13 ABC transporters, 2 Bin-amphiphysin-Rvs (BAR)-domain proteins, 95 major facilitator superfamily transporters, 24 protein kinases, 3 fas-

ciclins, 6 cutinases and 86 TFs with appressorium morphogenesis (Supplementary Table 3).

We next analysed 2,778 Pmk1-dependent, HP surface-independent genes. There was considerable overlap in predicted gene functions (Supplementary Table 3) but with changes associated with appressorium maturation, such as cytoskeletal remodelling genes encoding actin-binding proteins, cofilin, coronin, the F-actin capping protein Fes/CIP4 and EFC/F-BAR-domain proteins (Supplementary Fig. 5). Differential expression of septins and associated regulators was also observed (Supplementary Fig. 5b–d)[12,13]. Pmk1 therefore acts as a global regulator of the *M. oryzae* response to surface hydrophobicity, but its function clearly extends beyond initial development to appressorium maturation.

Defining the role of Mst12 in regulating appressorium gene expression. As Pmk1 is required for the expression of 6,333 genes during appressorium development, we identified downstream regulators to establish the hierarchy of genetic control. Mst12 has been reported to be regulated by Pmk1 (ref. [22]; Fig. 2a) but, unlike Δ*pmk1* mutants, Δ*mst12* mutants still form appressoria, although they cannot infect plants[22] (Extended Data Fig. 2a,b). To help define the function of Mst12, we carried out live-cell imaging and found the Δ*mst12* mutant impaired in its ability to undergo septin-dependent F-actin remodelling at the appressorium pore (Fig. 2b)[13]. Microtubules were disorganized in appressoria of the Δ*mst12* mutants (Fig. 2b) and, consistent with septin disorganization, the PAK-related kinase Chm1, ezrin/radixin/moesin protein Tea1, BAR domain-containing protein Rvs167, and staurosporine and temperature sensitive-4 (Stt4) lipid kinase (Fig. 2c)[12,13] were all mis-localized. Mst12 is therefore necessary for septin-dependent re-polarization of the appressorium and we thus performed comparative RNA-seq of the Δ*mst12* and Δ*pmk1* mutants (Supplementary Tables 4 and 5). This led to the identification of 2,512 DEGs in the Δ*mst12* mutant with significant changes in gene expression during conidial germination and, particularly after 8 h, during appressorium maturation (Fig. 2d). A set of 4,052 genes were also identified as Pmk1-dependent but Mst12-independent, with 2,281 genes regulated by both Pmk1 and Mst12 (Fig. 2e). Only 231 Mst12-dependent genes were Pmk1-independent (Fig. 2e). Appressorium-specific gene functions, such as melanin biosynthesis[27], were not expressed in the Δ*pmk1* mutants and delayed in expression in the Δ*mst12* mutants, consistent with delayed onset of appressorium formation compared with Guy11 (Extended Data Fig. 2c–f).

To investigate appressorium maturation, gene functions regulated by both Pmk1 and Mst12 were defined among the 2,281 DEGs. These included the cutinase gene family, implicated in plant infection[28] (Supplementary Fig. 6a–c), and a family of membrane-associated fasciclin glycoproteins involved in cell adhesion[29,30] (Supplementary Fig. 6d–g). Three fasciclins—Flp1 (MGG_02884), Flp2 (MGG_09372) and Flp3 (MGG_05483)—are present in *M. oryzae* and Flp1 plays a role in adhesion and pathogenicity[31]. A total of 436 genes predicted to encode secreted proteins[32] were also Pmk1- and Mst12-dependent, including seven known effector genes (Extended Data Fig. 3a–c), two of which, Bas2 and Bas3, have been reported to be Pmk1-dependent during invasive growth[15]. We therefore expressed Bas2p:green fluorescent protein (GFP) in a *pmk1*^{AS} mutant. This mutant allows conditional inactivation of the MAPK in the presence of the ATP analogue 1-naphthyl-PP1 (1NA-PP1; ref. [15]). When 1NA-PP1 was applied to the *pmk1*^{AS} mutant expressing Bas2pGFP, we observed a loss of Bas2–GFP fluorescence, suggesting that Pmk1 is necessary for its expression before plant infection (Extended Data Fig. 3d,e).

Given the significant effect of Mst12 on septin-dependent re-polarization—which is necessary for exocyst organization[25]—we reasoned that Δ*mst12* might be impaired in secretory functions. GFP fusion proteins of exocyst components were therefore expressed
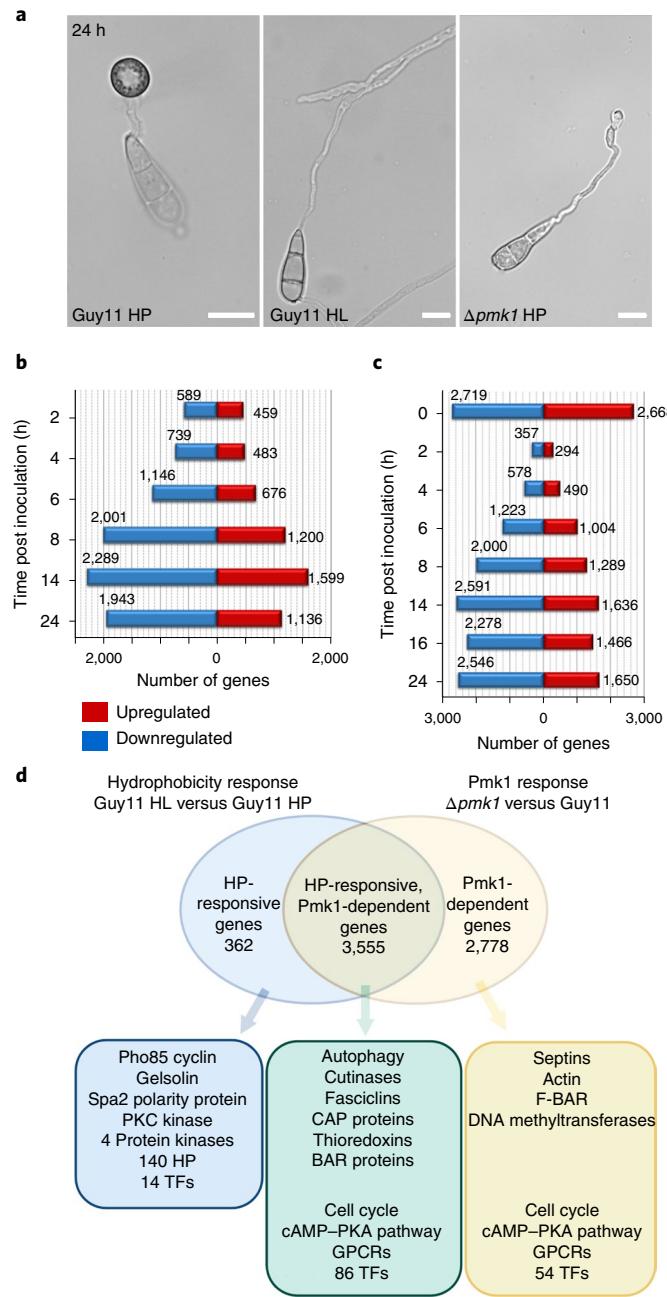
Fig. 1 | Global comparative transcriptional profile analysis to define the response of *M. oryzae* to surface hydrophobicity and the presence/absence of the Pmk1 MAPK. a, Bright-field microscopy to show germ-tube extension and appressorium formation of *M. oryzae* Guy11 on an HP (left) and an HL (middle) surface as well as a Δ*pmk1* mutant on an HP surface (right) 24 h after inoculation. Scale bars, 10 μm. **b**, Number of upregulated ($P_{adj} < 0.01$ and mod_lfc > 1) and downregulated ($P_{adj} < 0.01$ and mod_lfc < −1) genes in Guy11 in response to incubation on HL surfaces relative to HP surfaces between 2 and 24 h after inoculation. **c**, Number of upregulated ($P_{adj} < 0.01$ and mod_lfc > 1) and downregulated ($P_{adj} < 0.01$ and mod_lfc < −1) genes in a Δ*pmk1* mutant as compared with the wild-type Guy11 0–24 h after incubation on an HP surface. **d**, Venn diagram illustrating overlapping sets of genes with at least twofold differential expression in at least two time points ($P_{adj} < 0.01$ and mod_lfc > 1 or mod_lfc < −1) in Guy11 in response to incubation on HP or HL surfaces, or between the Δ*pmk1* mutant compared with Guy11 on an HP surface. Three distinct populations of genes were identified: HP-surface responsive only, HP-responsive and Pmk1-dependent, and Pmk1-dependent only. GPCRs, G protein–coupled receptors.

in Δ*mst12* and Guy11 *M. oryzae* (Extended Data Fig. 3f–k). In the Guy11 appressoria, exocyst components form a ring structure that is absent in the Δ*mst12* mutants (Extended Data Fig. 3f–k). We conclude that Pmk1 and Mst12 are necessary for the expression of genes involved in cytoskeleton reorientation, exocyst and effector functions during plant tissue invasion.

We used chromatin immunoprecipitation with sequencing (ChIP–seq) to identify direct targets of Mst12. A functional Mst12–GFP fusion protein was expressed in a Δ*mst12* strain, which complemented the mutant phenotype and localized to the appressorium nucleus (Extended Data Fig. 4a,b). Cross-linked chromatin was isolated from mycelium, followed by immunoprecipitation and sequencing of Mst12–GFP-bound genomic DNA. ChIP–seq identified 1,596 broad peaks within ±2 kb of 726 genes (Supplementary Table 6), which defined 113 downregulated and 65 upregulated genes (Fig. 2f and Extended Data Fig. 4c). We calculated the number of Mst12-dependent genes (based on RNA-seq analysis during appressorium development) that were direct ChIP–seq-defined targets of Mst12. This revealed a considerable overlap of 113 genes directly controlled by Mst12 (Fig. 2g). Among these, 25 genes encode putative secreted proteins, such as the SET domain (PF00856) containing the protein-encoding gene *MCG1* (MGG_00339)[33] and a secreted catalase (MGG_06442)[34] (Supplementary Table 6). We predicted consensus binding motifs from peak sequences obtained by ChIP–seq analysis identifying five over-represented motifs in these sequences (Fig. 2h). We found that Motifs 1–3 were over-represented ($P < 0.001$) in the promoters of the Mst12-dependent genes identified by RNA-seq. For example, Motif 1 was present in 609 of 1,848 genes (32.95%) downregulated in the Δ*mst12* mutants during appressorium development (Extended Data Fig. 4d). The Mst12 targets include genes reported to play roles in appressorium maturation and plant infection (Supplementary Table 6). Rvs167 (ref. [13]), for example, is an Mst12 target (Fig. 2i), consistent with its mis-localization in Δ*mst12* appressoria (Fig. 2c) and differential gene expression (Supplementary Table 6). Similarly, the 1,3,6,8-tetrahydroxynaphthalene reductase-encoding gene *4HNR*, involved in melanin biosynthesis[35], is an Mst12 target (Fig. 2i) and downregulated in Δ*mst12* mycelium (Supplementary Fig. 7). Comparative ChIP–seq and RNA-seq analysis therefore provided evidence that Mst12 regulates cellular functions associated with appressorium maturation.

Identification of the hierarchy of transcriptional regulation required for appressorium development by *M. oryzae*. As Mst12 regulates a subset of genes associated with appressorium re-polarization, we reasoned that Pmk1 must regulate additional TFs, including some acting earlier during development. We therefore determined the total number of putative TF-encoding genes that were differentially regulated by at least twofold ($P_{adj} < 0.01$ and mod_lfc > 1 or mod_lfc < −1) in at least two time points in the Δ*pmk1* and/or Δ*mst12* mutants compared with Guy11 *M. oryzae*. We found 140 such TF genes, of which 95 were expressed during appressorium morphogenesis and Pmk1-dependent, with 45 associated with the later stages of appressorium maturation and dependent on both Pmk1 and Mst12 (Fig. 3a). We plotted heatmaps for each gene set (Fig. 3b–d), which revealed a clade of 15 TF-encoding genes severely downregulated in the Δ*pmk1* mutant, which we called Clade 4 (Fig. 3c and Supplementary Table 7). This includes nine Zn₂Cys₆ TFs, some of which were previously implicated in stress responses (Fzc64, Fzc52, Fzc41 and Fzc30), conidial germination (Fzc50) and appressorium formation (Fzc75)[36]. Five Clade 4 TFs were uncharacterized and named *RPP* genes (for related to the Pmk1 pathway): *RPP1* (MGG_10212), *RPP2* (MGG_09276), *RPP3* (MGG_07218), *RPP4* (MGG_07368) and *RPP5* (MGG_08917). Clade 4 also includes the *PIG1* TF gene (MGG_07215), previously reported to regulate melanin biosynthesis[37], *ALCR* (MGG_02129),

a homologue of *AlcR* from *Aspergillus nidulans* responsible for the activation of ethanol utilization[38] and the homeobox-domain TF gene *HOX7* (MGG_12865), involved in appressorium formation[39]. These TF genes were downregulated in a Δ*pmk1* mutant from 4 h (Fig. 3e)—the time when an appressorium first develops—and altered in expression in Δ*mst12* mutants at later time points, consistent with its delay in appressorium formation (Fig. 3f).

To test whether Clade 4 TF genes play important roles in appressorium development, we generated Δ*alcR*, Δ*rpp1*, Δ*rpp2*, Δ*rpp4*, Δ*rpp5*, Δ*rpp3*, Δ*rpp3*Δ*pig1* and Δ*hox7* mutants in either Δ*ku70* (a mutant of Guy11 lacking non-homologous DNA end-joining to facilitate homologous recombination[6]) or Guy11 (Supplementary Fig. 7). A double mutant of *RPP3* and *PIG1* was also made, because they are part of a gene cluster on chromosome 2 associated with melanin biosynthesis, including *BUF1* and *4HNR*[40], and we reasoned that the TFs might have overlapping functions. We inoculated 21-day-old seedlings of the blast-susceptible rice cultivar CO-39 with conidial suspensions of each mutant and quantified disease symptoms after 5 d (Fig. 3g,h and Extended Data Fig. 5). Guy11 and Δ*ku70* were able to cause plant infection but, by contrast, the Δ*hox7* mutant was non-pathogenic[39] (Fig. 3g), while both the Δ*rpp3* and Δ*rpp3*Δ*pig1* mutants were reduced in virulence. Conversely, the Δ*aclR* mutant caused slightly more blast lesions than Guy11 (Fig. 3g,h).

The Hox7 homeobox TF is regulated by the Pmk1 MAP kinase. To investigate the role of Clade 4 TFs in pathogenesis, we tested whether mutants could form appressoria (Extended Data Fig. 5b). All mutants made appressoria normally, except the Δ*hox7* mutants, which formed immature non-melanised terminal swellings that re-germinated into hypha-like structures (Fig. 4a and Extended Data Fig. 6a,b). Because the loss of *HOX7* affected appressorium development, we hypothesized it might act distinctly to Mst12 and other Clade 4 TFs. Hox7 is one of six homeobox-domain (PF00046) TFs and two homeobox KN domain (PF05920)-encoding genes previously identified, but its relationship to Pmk1 is unknown[39]. We therefore carried out comparative RNA-seq of Δ*hox7* with the Δ*pmk1* and Δ*mst12* mutants at 14 h on HP surfaces (Fig. 4b and Supplementary Table 8,9). Hox7 controls the expression of 4,211 genes, of which 2,332 are downregulated ($P_{adj} < 0.01$ and mod_lfc < −1) and 1,879 upregulated ($P_{adj} < 0.01$ and mod_lfc > 1; Extended Data Fig. 6b). We then identified sets of overlapping genes in the Δ*hox7*, Δ*pmk1* and Δ*mst12* mutants showing differential expression compared with Guy11 (Fig. 4b). Pmk1 and Hox7 shared 1,942 DEGs, whereas Mst12 and Hox7 shared only 169 DEGs (Fig. 4b). Our analysis revealed 709 DGEs in the Δ*pmk1*, Δ*mst12* and Δ*hox7* mutants, with a very high level of similarity between the Δ*pmk1* and Δ*hox7* mutants, in contrast to Δ*mst12* (Extended Data Fig. 6c). We therefore reasoned that Hox7 might act downstream of Pmk1 to

regulate such a strongly overlapping set of genes. To test this idea, we investigated the expression of Clade 4 TFs and found that the gene expression patterns were similar between the Δ*pmk1* and Δ*hox7* mutants (Fig. 4c). Widening our analysis to the 1,942 genes that were differentially regulated by both Pmk1 and Hox7 revealed a strongly overlapping pattern of transcriptional regulation (Extended Data Fig. 6d). For example, Pmk1 and Hox7 are both required for the regulation of the RAM pathway, melanin biosynthesis, autophagy and cell-cycle control genes (Extended Data Fig. 6e). Expression of the cyclin genes *Cln3*, *Clb2* and *Clb3*; CDK-related genes *Mih1*, *Cdc28*, *Swe1* and *Cks1*; and the DNA damage response pathway-related genes *Cds1*, *Dun1* and *Chk1* (Extended Data Fig. 6f) as well as autophagy genes (Extended Data Fig. 6g) are mis-regulated in Δ*hox7* mutants. To investigate the role of Hox7 in cell-cycle control and autophagy, we introduced a Histone H1-red fluorescent protein (RFP) nuclear marker into Guy11 and Δ*pmk1* M. oryzae and a H1–GFP marker into the Δ*mst12* and Δ*hox7* mutants, and monitored the nuclear numbers for 24 h following conidial germination (Fig. 4d). The Δ*hox7* mutant contained >4 nuclei by 24 h, resembling Δ*pmk1*, whereas the Δ*mst12* mutant resembled Guy11 with a single nucleus in the appressorium. Hox7 may therefore be required for cell-cycle arrest in the apical cell of the conidium after mitosis and migration of daughter nuclei to the incipient appressorium and conidial cell, respectively[7]. Furthermore, conidia of both the Δ*hox7* and Δ*pmk1* mutants did not collapse due to autophagy by 24 h, as observed in Guy11 and Δ*mst12*, consistent with the regulation of autophagy requiring both Pmk1 and Hox7.

A TOR kinase-dependent nutrient-sensing pathway has recently been shown to be required for appressorium morphogenesis, including cell-cycle arrest before infection, cell development and the onset of autophagy. This metabolic checkpoint is downstream of PKA but may act upstream of Pmk1 (refs. [9–11]). We decided to test whether the metabolic checkpoint affects the action of Pmk1 and Hox7. First, we tested whether the Δ*pmk1* and Δ*hox7* mutants were responsive to cAMP. The Δ*pmk1* mutant responded to exogenous cAMP treatment by undergoing increased hooking, as reported previously[17], as well as reduced conidial germination, whereas Δ*hox7* developed multiple aberrant non-melanised swellings and showed less hyphal-like growth. Pmk1 and Hox7 therefore seem to act downstream of cAMP–PKA signalling (Supplementary Fig. 8). We next tested whether inhibition of TOR might be compromised in the Δ*pmk1* and Δ*hox7* mutants, thereby explaining their inability to make appressoria and undergo autophagy. Spores of Guy11 M. oryzae and Δ*pmk1* and Δ*hox7* mutants were subject to forced inactivation of TOR with rapamycin. This treatment did not restore appressorium development or inhibit multiple nuclear divisions in the Δ*pmk1* mutants, consistent with previous observations[10], but also had no effect on the Δ*hox7* mutants, suggesting that

Fig. 2 | Functional analysis and comparative global transcriptional profile analysis in response to the presence/absence of the *M. oryzae* TF Mst12. a, Schematic representation of the Pmk1 MAPK signalling pathway in *M. oryzae*. Dissociation of Mgb1 causes activation of Mst11 (MAPKKK), which activates Mst7 (MAPKK) and ultimately Pmk1 (MAPK). The MAPK signalling complex is scaffolded by Mst50. Mst7 activates Pmk1, which regulates a series of uncharacterized TFs as well as Mst12 (refs. [69,70]). **b**, Live-cell images showing the cellular localization of Lifeact–RFP, Sep3–GFP and β-tubulin–GFP in an appressorium pore of Guy11 and Δ*mst12* following incubation on an HP surface for 24 h. **c**, Micrographs showing the cellular localization of Chm1–GFP, Tea1–GFP, Rvs167–GFP and Stt4–GFP in appressorium pores of Guy11 and Δ*mst12* following incubation on an HP surface for 24 h. **b,c**, Scale bars, 10 μm. **d**, Number of upregulated ($P_{adj} < 0.01$ and mod_lfc > 1) and downregulated ($P_{adj} < 0.01$ and mod_lfc < −1) genes in a Δ*mst12* mutant as compared with Guy11 at different time points (0–24 h) following incubation on an HP surface. **e**, Venn diagram illustrating overlapping sets of DGEs with at least twofold differential expression in at least two time points ($P_{adj} < 0.01$ and mod_lfc > 1 or mod_lfc < −1) between a Δ*pmk1* mutant and Guy11 and a Δ*mst12* mutant versus Guy11, all incubated on an HP surface. Three distinct populations of genes were identified: Pmk1-dependent only, Pmk1- and Mst12-dependent, and Mst12-dependent only. **f**, Number of genes that were downregulated ($P_{adj} < 0.01$ and mod_lfc < -1), upregulated ($P_{adj} < 0.01$ and mod_lfc > 1) or bound by Mst12 during mycelium growth (determined by ChIP-seq; two biological replicates) **g**, Number of genes that were differentially regulated (downregulated ($P_{adj} < 0.01$ and mod_lfc < −1) and upregulated ($P_{adj} < 0.01$ and mod_lfc > 1)) or bound by Mst12 during appressorium development (determined by ChIP-seq; two biological replicates). **h**, Consensus DNA-binding motifs, predicted using MEME, for the TF Mst12 based on ChIP-seq. **i**, Representative raw ChIP-seq peaks and RNA-seq for the BAR domain–encoding gene (PF03114) *RVS167* (MGG_11497; left) and the tetrahydroxynaphthalene reductase–encoding gene *4HNR* (MGG_07216; right). The blue boxes indicate peaks identified by MACS2 using ChIP-seq analysis.

Pmk1 and Hox7 are not influenced by TOR activity (Supplementary Fig. 9). The TOR-dependent metabolic checkpoint has been reported to lead to a G2 arrest before appressorium morphogenesis[9,11]; we thus tested whether a forced G2 arrest in response to treatment with the microtubule polymerization inhibitor benomyl would restore appressorium development to the Δpmk1 and Δhox7 mutants. Benomyl treatment did not restore appressorium

formation or autophagy to either mutant or affect subsequent nuclear divisions (Supplementary Fig. 10a,b). Our results therefore indicate that Pmk1 and Hox7 act downstream of the cAMP–PKA pathway but are not dependent on the TOR-dependent metabolic checkpoint. This emphasises both the central role of Pmk1 as a global regulator of appressorium development by *M. oryzae*[15] and its close relationship to Hox7.
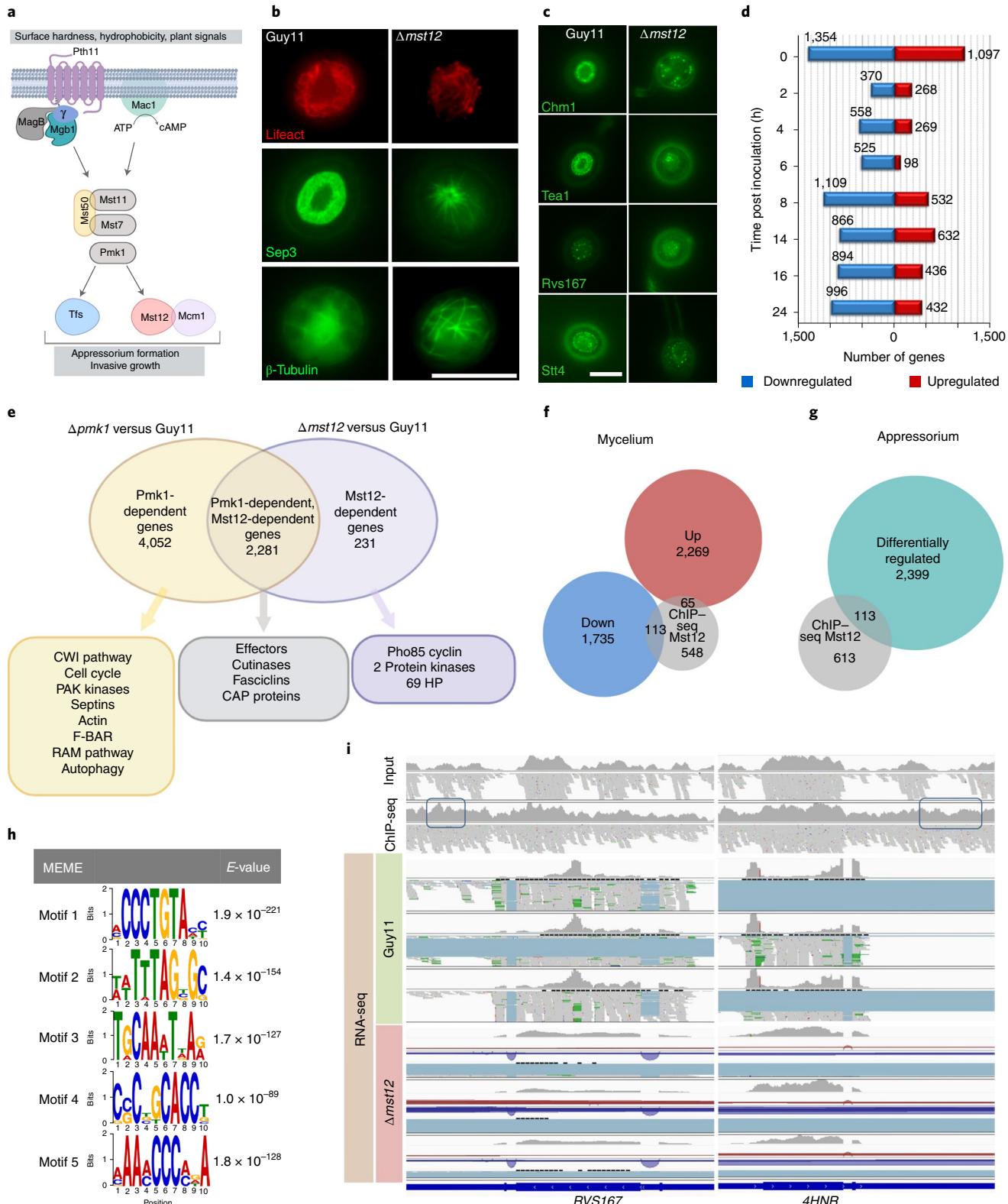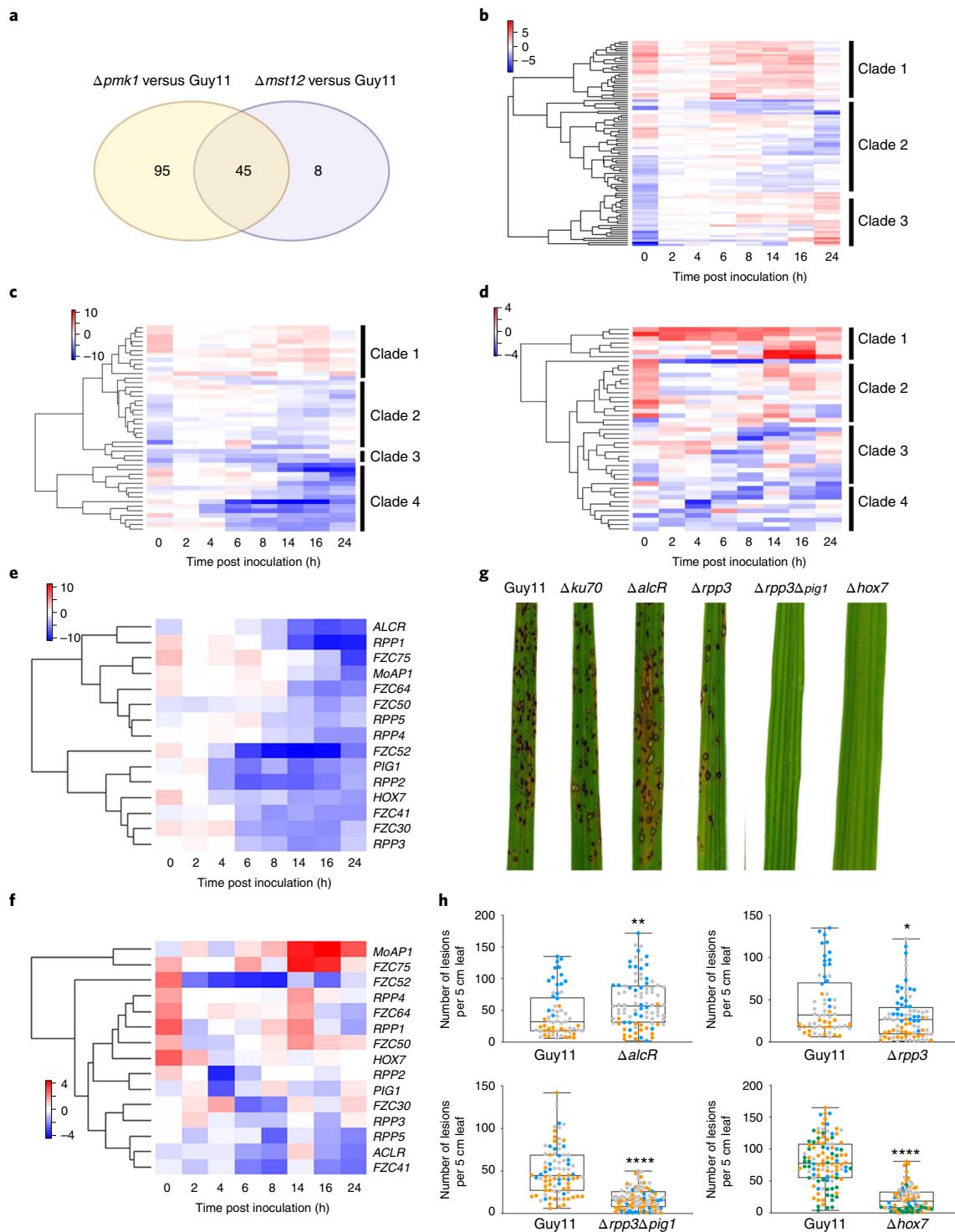
We carried out ChIP–seq analysis to identify targets of the TF Hox7. A functional Hox7–3×FLAG fusion protein was expressed in Δ*hox7*, which fully complemented its phenotype (Extended Data Fig. 7). Cross-linked chromatin was isolated from mycelium, followed by immunoprecipitation and sequencing of Hox7–3×FLAG-bound genomic DNA. ChIP–seq identified 242 broad peaks ±2 kb of 238 genes (Supplementary Table 10), which defined 15 downregulated and 66 upregulated genes during mycelium growth and 33 downregulated and 56 upregulated genes during appressorium development (Fig. 4e,f and Extended Data Fig. 7d). Among the Hox7 targets were three Clade 4 TFs—*FZC64* (MGG_00320) and *FZC52* (MGG_09676)[36],

and *RPP3* (MGG_07218)—consistent with Hox7 acting within a transcriptional hierarchy during appressorium morphogenesis. The melanin biosynthetic genes *RSY1* (MGG_05059), required for appressorium function[27], and *RTT109* encoding a H3K56 histone acetylation protein involved in pathogenicity[41] were also identified. Five over-represented consensus motifs within peak sequences were predicted by ChIP–seq (Fig. 4h). Motifs 1–5 were over-represented ($P < 0.001$) in Hox7-dependent DEGs, as identified by RNA-seq. Motif 2 was present in 1,989 of 2,332 Hox-dependent genes (85.29%) during appressorium development (Extended Data Fig. 7e). Targets of Hox7 included a basic Helix Loop Helix TF gene, MGG_10575,

Fig. 3 | Defining the hierarchy of transcriptional control during appressorium development by *M. oryzae*. a, Venn diagram showing overlapping sets of *M. oryzae* putative TF-encoding genes with at least twofold differential expression between Δ*pmk1* and Guy11; Δ*mst12* and Guy11; and Δ*pmk1*, Δ*mst12* and Guy11 in at least two time points ($P_{adj} < 0.01$ and mod_lfc > 1 or mod_lfc < −1). **b**, Heatmap showing the temporal pattern of the relative transcript abundance of 95 TF-encoding genes between Δ*pmk1* and Guy11. **c**, Heatmap showing the temporal pattern of the relative transcript abundance of 45 TF-encoding genes between Δ*pmk1* and Guy11. **d**, Heatmap showing the temporal pattern of the relative transcript abundance of 53 TF-encoding genes between Δ*mst12* and Guy11. **e**, Heatmap showing the temporal pattern of the transcript abundance of Clade 4 TF-encoding genes that are differentially regulated in Δ*pmk1* as compared with Guy11. **f**, Heatmap showing the temporal pattern of the transcript abundance of Clade 4 TF-encoding genes that are differentially regulated in Δ*mst12* as compared with Guy11. **b–f**, Genes that are downregulated in the mutant are shown in blue and those that are upregulated in red. **g**, Rice blast disease symptoms of the Δ*alcR*, Δ*rpp3*, Δ*rpp3*Δ*pig1* and Δ*hox7* mutants as compared with Guy11 and a Δ*ku70* mutant. Rice seedlings of cultivar CO-39 were spray-inoculated with conidial suspensions of equal concentrations of each *M. oryzae* strain and incubated for 5 d. **h**, Number of rice blast disease lesions generated per 5 cm leaf in pathogenicity assays. Box-and-whisker plots with individual data points (data points of different colours represent different biological replicates); the boxes show the 25th and 75th percentiles, the median is indicated by a horizontal line and the minimum and maximum values by the ends of the whiskers. A two-tailed non-parametric Mann–Whitney test was conducted; Δ*alcR* versus Guy11, **P = 0.0017, *n* = 3 biological replicates; Δ*rpp3* versus Guy11, *P = 0.0131, *n* = 3 biological replicates; Δ*rpp3*Δ*pig1* versus Guy11, ****P < 0.0001, *n* = 3 biological replicates; and Δ*hox7* versus Guy11, ****P < 0.0001, *n* = 4 biological replicates.

homologous to *Candida albicans CPH2* (4×10^{-22}), involved in hyper-filamentous growth and hyphae development[42] and a RAN1/PAT1 kinase gene (MGG_05074)-similar mammalian gene required for cell-cycle progression and meiotic development[43] (Fig. 4g).

Hox7 is a direct target of the Pmk1 MAP kinase in *M. oryzae*. To understand how Pmk1 regulates Hox7, we carried out exploratory and quantitative phosphoproteomic analyses. Phosphoproteins were purified from Δ*pmk1*, Δ*hox7* and Guy11 at 6 h following conidial germination and analysed by liquid chromatography with tandem mass spectrometry (LC–MS/MS). This revealed Pmk1-dependent phosphorylation of proteins associated with cell-cycle control—including Dun1 and Far1—the autophagy-related proteins Atg13 and Atg26, and eight components of the cAMP–PKA pathway[44,45]. A subset of phosphoproteins were also dependent on the presence of Hox7 (Fig. 5a).

Importantly, phosphorylation of Hox7 was detected at a proline-directed serine residue at position 158 within a PxSP MAP kinase motif, and two other residues, S126 and S254 (Fig. 5a and Extended Data Fig. 8). These serine residues, especially S158, were conserved among putative Hox7 orthologues in many filamentous fungi, but not yeast, species (Extended Data Fig. 8). To test whether phosphorylation of S126, S158 and S254 was Pmk1-dependent, parallel reaction monitoring (PRM) was performed in both Guy11 *M. oryzae* and Δ*pmk1* mutants (Supplementary Table 11). The PRM showed that the relative normalized intensity of peptides associated with S126 and S158 of Hox7 was reduced in Δ*pmk1* compared with Guy11 (Fig. 5b,c). We therefore decided to carry out PRM using the *pmk1*^{AS} mutant in which MAPK activity could be inhibited with 1NA-PP1. Conidia of the *pmk1*^{AS} mutant were germinated on an HP surface and treated with 1NA-PP1. Phosphoproteins were extracted at 2, 3 and 4 h following treatment with or without 1NA-PP1 (Fig. 5d) and the relative normalized intensity of peptides associated with S126 (Fig. 5f), S158 (Fig. 5g) and S254 (Fig. 5h) of Hox7 was

measured. There was a maximum intensity value at 3–4 h for the three peptides in the absence of NA-PP1 (Fig. 5f–h) but the relative normalized intensity of peptides was reduced ($P < 0.01$) in the presence of NA-PP1 (when Pmk1 is inactive), providing evidence that phosphorylation of S158 in particular depends on Pmk1, either directly or indirectly. We carried out an identical experiment in which 1NA-PP1 was added at later time points (4 h) to define the window of Pmk1-dependent phosphorylation of Hox7. The normalized intensity of phosphopeptides was reduced following Pmk1 inhibition (Extended Data Fig. 9) but less pronounced than in the original experiment (Fig. 5d–h), consistent with Pmk1-dependent phosphorylation of S158 of Hox7 occurring within the first 3–4 h of conidial germination.
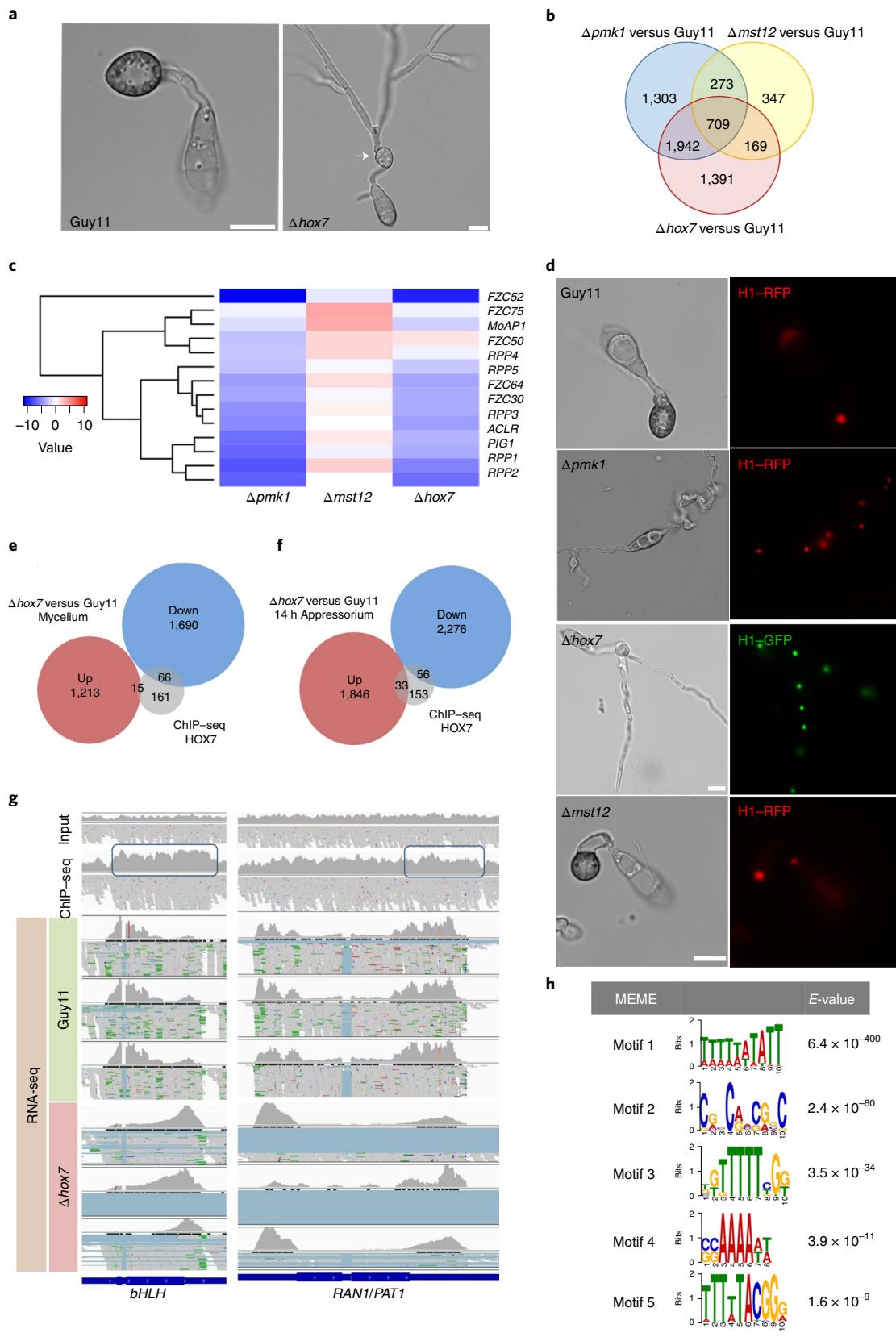
To determine whether Pmk1 phosphorylates Hox7, we carried out an in vitro kinase assay, followed by LC–MS/MS. We expressed and purified 6×His–glutathione-*S*-transferase (GST)–Pmk1 (GST–Pmk1), 6×His–small ubiquitin-like modifier (SUMO)–Mst12 (SUMO–Mst12) and 6×His–maltose-binding protein (MBP)–Hox7t-342 proteins from *Escherichia coli* and incubated them in the presence of a recombinant, constitutively active MAPKK from tobacco (*Nicotiana tabacum*)[46] called MEK2^{DD} (Fig. 6), which specifically activates Pmk1 in a pTEpY motif (see Extended Data Fig. 10b). When MEK2^{DD}-activated GST–Pmk1 was incubated in the presence of SUMO–Mst12 we reproducibly detected phosphorylation at S133 of Mst12 within a MAP kinase motif PxSP (Fig. 6). Other phosphoproteins of Mst12 were also observed but consistent spectral counts were found for S133 (see Supplementary Table 12). This provides evidence that MEK2^{DD} activates 6×His–GST–Pmk1, which enables Pmk1 to phosphorylate its targets, including Mst12. We were also able to detect phosphorylation of Hox7 and reproducibly identify a peptide associated with S158 (Fig. 6) as the clearest outcome of Pmk1-dependent phosphorylation, consistent with discovery phosphoproteomics and PRM experiments. We conclude that Pmk1 can phosphorylate Mst12 at S133 and Hox7 at S158, both of which occur within MAPK motifs .

Fig. 4 | Characterization of the Hox7 homeobox TF and its role in the regulation of gene expression during appressorium development by *M. oryzae*.
a, Bright-field microscopy of appressorium development by Guy11 and a Δ*hox7* mutant following incubation on an HP surface for 24 h. The arrow points to re-germination of an incipient appressorium and hyphal elongation. **b**, Venn diagram showing overlapping sets of genes with at least twofold difference ($P_{adj} < 0.01$ and mod_lfc > 1 or mod_lfc < −1) between Guy11 and the Δ*pmk1*, Δ*mst12* and Δ*hox7* mutants, respectively, during 14 h of appressorium development. **c**, Heatmap showing the relative transcript abundance of Clade 4–associated TF genes in the Δ*pmk1*, Δ*mst12* and Δ*hox7* mutants as compared with Guy11. **d**, Live-cell images showing nuclear dynamics in Guy11 and the Δ*pmk1*, Δ*hox7* and Δ*mst12* mutants, each expressing H1-RFP or H1-GFP, after 24 h germination on an HP surface. **a,d**, Scale bars, 10 μm. **e**, Number of genes that were downregulated ($P_{adj} < 0.01$ and mod_lfc < −1), upregulated ($P_{adj} < 0.01$ and mod_lfc > 1) or bound by Hox7 (grey) during mycelium growth (determined by ChIP–seq; three biological replicates). **f**, Number of genes that were downregulated ($P_{adj} < 0.01$ and mod_lfc < −1), upregulated ($P_{adj} < 0.01$ and mod_lfc > 1) or bound by Hox7 (grey) during appressorium development at 14 h (determined by ChIP–seq; three biological replicates). **g**, Representative raw ChIP–seq peaks and RNA-seq for the basic Helix Loop Helix TF gene (*bHLH*; MGG_10575) homologous to *C. albicans HMS1* and the *RAN1/PAT1* kinase gene (MGG_05074). The blue boxes represent the peaks identified by MACS2 using ChIP–seq analysis. **h**, Consensus DNA-binding motifs, predicted using MEME, for the TF Hox7 based on ChIP–seq analysis.

Pmk1-dependent Hox7 phosphorylation is necessary for appressorium development. To determine the physiological relevance of Hox7 phosphorylation, alleles of Hox7 were generated with serine–alanine substitutions to prevent phosphorylation and serine–aspartate substitutions to mimic phosphorylation. These were expressed in a $\Delta hox7$ mutant. Conidia of Guy11, $\Delta hox7$, a $\Delta hox7$:TrpC-Hox7 strain complemented with the wild-type $HOX7$ allele, the phospho-dead $\Delta hox7$:$TrpCp$-$Hox7^{S126A\text{-}S158A\text{-}S254A}$ mutant and the phosphomimetic $\Delta hox7$:$TrpCp$-$Hox7^{S126D\text{-}S158D\text{-}S254D}$ mutant were inoculated on HP surfaces. We then evaluated their ability to

a

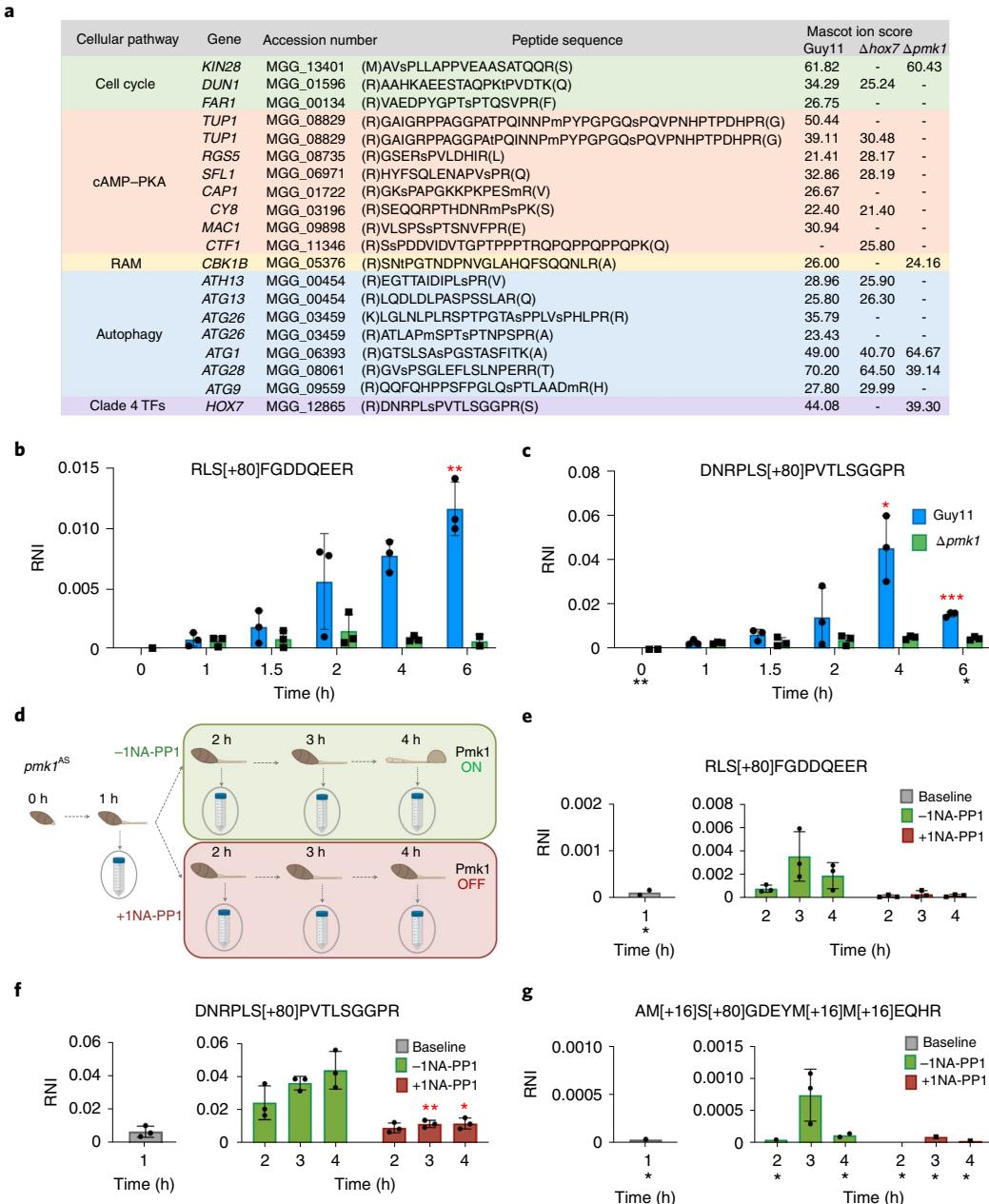| Cellular pathway	Gene	Accession number	Peptide sequence	Mascot ion score		
				Guy11	Δ*hox7*	Δ*pmk1*
Cell cycle	*KIN28*	MGG_13401	(M)AVsPLLAPPVEAASATQQR(S)	61.82	-	60.43
	DUN1	MGG_01596	(R)AAHKAEESTAQPKtPVDTK(Q)	34.29	25.24	-
	FAR1	MGG_00134	(R)VAEDPYGPTsPTQSVPR(F)	26.75	-	-
cAMP–PKA	*TUP1*	MGG_08829	(R)GAIGRPPAGGPATPQINNPmPYPGPGQsPQVPNHPTPDHPR(G)	50.44	-	-
	TUP1	MGG_08829	(R)GAIGRPPAGGPAtPQINNPmPYPGPGQsPQVPNHPTPDHPR(G)	39.11	30.48	-
	RGS5	MGG_08735	(R)GSERsPVLDHIR(L)	21.41	28.17	-
	SFL1	MGG_06971	(R)HYFSQLENAPVsPR(Q)	32.86	28.19	-
	CAP1	MGG_01722	(R)GKsPAPGKKPKPESmR(V)	26.67	-	-
	CY8	MGG_03196	(R)SEQQRPTHDNRmPsPK(S)	22.40	21.40	-
	MAC1	MGG_09898	(R)VLSPSsPTSNVFPR(E)	30.94	-	-
	CTF1	MGG_11346	(R)SsPDDVIDVTGPTPPPTRQPQPPQPPQPK(Q)	-	25.80	-
RAM	*CBK1B*	MGG_05376	(R)SNtPGTNDPNVGLAHQFSQQNLR(A)	26.00	-	24.16
Autophagy	*ATH13*	MGG_00454	(R)EGTTAIDIPLsPR(V)	28.96	25.90	-
	ATG13	MGG_00454	(R)LQDLDLPASPSSLAR(Q)	25.80	26.30	-
	ATG26	MGG_03459	(K)LGLNLPLRSPTPGTAsPPLVsPHLPR(R)	35.79	-	-
	ATG26	MGG_03459	(R)ATLAPmSPTsPTNPSPR(A)	23.43	-	-
	ATG1	MGG_06393	(R)GTSLSAsPGSTASFITK(A)	49.00	40.70	64.67
	ATG28	MGG_08061	(R)GVsPSGLEFLSLNPERR(T)	70.20	64.50	39.14
	ATG9	MGG_09559	(R)QQFQHPPSFPGLQsPTLAADmR(H)	27.80	29.99	-
Clade 4 TFs	*HOX7*	MGG_12865	(R)DNRPLsPVTLSGGPR(S)	44.08	-	39.30

Fig. 5 | Phosphoproteomic analysis reveals Pmk1-dependent phosphorylation of Hox7 in *M. oryzae*. a, Classification of phosphoproteins identified by discovery phosphoproteomics in Guy11 and the Δ*pmk1* and Δ*hox7* mutants at 6 h of appressorium development on an HP surface. The specific peptide sequence containing proline-directed phosphorylation either at a serine or threonine residue (lowercase 's' and 't') for each accession number is shown with the corresponding Mascot ion score. **b**, Relative normalized intensity (RNI), determined by PRM, of the peptide associated with phosphorylated S126 of Hox7 during appressorium development up to 6 h after conidial germination in Guy11 *M. oryzae* and the Δ*pmk1* mutant. **P = 0.0088 (6 h). **c**, RNI of the peptide associated with phosphorylated S158 of Hox7 during appressorium development up to 6 h after conidial germination in Guy11 and Δ*pmk1*, determined by PRM. *P = 0.0418 (4 h) and ***P = 0.0004 (6 h). **d**, Experimental design for PRM to measure the RNI of peptides associated with the S126, S158 and S254 residues in Hox7. The *pmk1*^AS conditional mutant was incubated on an HP surface for 1 (baseline), 2, 3 and 4 h in the presence or absence of the ATP analogue 1NA-PP1 (+1NA-PP1 and −1NA-PP1, respectively). Falcon tubes represent sample collection. **e**, RNI of the peptide associated with phosphorylated S126 of Hox7 during appressorium development in *pmk1*^AS conditional mutant ±1NA-PP1, determined by PRM. **f**, RNI of peptide associated with phosphorylated S158 of Hox7 during appressorium development in *pmk1*^AS conditional mutant in ±1NA-PP1, determined by PRM. **P = 0.0027 (3 h) and *P = 0.0315 (4 h). **g**, RNI of the peptide associated with phosphorylated S254 of Hox7 during appressorium development in the *pmk1*^AS conditional mutant ±1NA-PP1, determined by PRM. **b,c,e–g**, Data are the mean ± s.d.; n = 3 biological replicates with one (**b,e–g**) or two (**c**) technical replicates per biological replicate. Black asterisks indicate that some peptides could not be detected in one or more biological replicates; red asterisks indicate significant P values.

form appressoria after 24 h. The phospho-dead Δ*hox7:TrpCp-Hox7*^S126A-S158A-S254A mutant was unable to develop appressoria and instead formed re-germinated terminal swellings. By contrast, the phosphomimetic Δ*hox7:TrpCp-Hox7*^S126D-S158D-S254D mutant was able to develop melanised appressoria but also exhibited a diverse set of other morphologies, which also varied among individual transformants

	Hox7								Mst12							
	MBP–Hox7t–342		MEK2DD and MBP–Hox7t–342		GST–Pmk1 and MBP–Hox7t–342		MEK2DD and GST–Pmk1 and MBP–Hox7t–342		SUMO–Mst12		MEK2DD and SUMO–Mst12		GST–Pmk1 and SUMO–Mst12		MEK2DD and GST–Pmk1 and SUMO–Mst12	
	Rep1	Rep2	Rep1	Rep2	Rep1	Rep2	Rep1	Rep2	Rep1	Rep2	Rep1	Rep2	Rep1	Rep2	Rep1	Rep2
SUMO–Hox7t-342																
(R)DNRPL[pS]PVTLSGGPR (S158)																
S6/7: phospho (+79.97)					2	2	6	7								
(R)DNRPLSPV[pT]LSGGPR																
T9/10: phospho (+79.97)							2	1								
LRVIPQDGQTSTPSSTTSPISGPPG[pT]L[pT]PPE[pY]VHSP[pTS]QNK(R)																
T26: phospho (+79.97)							1									
T28: phospho (+79.97)							1									
Y32: phospho (+79.97)								2								
S38: phospho (+79.97)								1								
T37: phospho (+79.97)								1								
LYTSQSQA[pY]QR																
Y9: phospho (+79.97)					1											
SNSPTMSTLAMAAP[pS]PHAPFKK																
S15: phospho (+79.97)								1								
SSTSDSWAGS[pS]RT[pS]PFLPGTSTSTLR																
S11: phospho (+79.97)								2								
S14: phospho (+79.97)								1								
TSPFLPGTSTSTLR[pS]PAAIEQNDPMDR																
S15: phospho (+79.97)								1								
S15: phospho (+79.97), m25: oxidation (+15.99)							2									
VIPQDGQTSTPSSTTSPISGPPGTLTPPEYVHSPT[pS]QNKR																
S36: phospho (+79.97)								1								
MBP–Mst12																
SGTDASLEEPK[pS]PFLDFLYK (S133)																
S12: phospho (+79.97)															4	2
HAS[M]PAYGLEYSPAP[pS]FVSSHYDDYGNR																
M4: oxidation (+15.99), s16: phospho (+79.97)															1	
[pS]A[pT]VMGSEVGPYPQK																
S1: phospho (+79.97)											1					
S1: phospho (+79.97), m5: oxidation (+15.99)											1				1	
T3: phospho (+79.97)											1					
T3: phospho (+79.97), m5: oxidation (+15.99)											1				1	

Fig. 6 | Purified recombinant GST–Pmk1 phosphorylates MBP–Hox7 and SUMO–Mst12 in vitro. MBP–Hox7 and SUMO–Mst12 were incubated with or without GST–Pmk1 and 6×His-tagged MEK2DD in the presence of 1 μM ATP for 30 min, as indicated in each column. Phosphorylated peptides were identified by LC–MS/MS and the spectra were manually inspected. MEK2DD phosphorylates the activation loop of Pmk1 in vitro, activating the Pmk1 kinase activity (see Supplementary Table 13). Activated purified GST–Pmk1 phosphorylates multiple residues on MBP–Hox7t-342 and SUMO–Mst12 TFs, including sites in the PxSP motifs identified in vivo. Phosphopeptides are shown with modified residues in red, and phosphorylation is shown as pS or pT in brackets (+79.97 Da) and oxidized methionine by M (+15.99 Da). Spectral counts are shown from two technical replicates (Rep1 and Rep2), with the position of the modified residue indicated. MBP–Hox7t-342, His-tagged MBP–Hox7 truncated (Met1-Q342) fusion protein.

(Extended Data Fig. 10). Hox7 phosphorylation by Pmk1 is therefore necessary for its function during appressorium development by *M. oryzae*.

Discussion

In this study we have identified the global transcriptional signature associated with appressorium development by *M. oryzae* in response to surface hydrophobicity and used comparative transcriptome analysis to define a hierarchy of Pmk1-dependent TFs necessary for appressorium morphogenesis. Collectively, this has enabled formulation of the model presented in Fig. 7c.

The TF Hox7 emerges from this study as an important regulator of appressorium development. Hox7 was previously reported to be necessary for plant infection[39] but its function was unknown. Based on phosphoproteomic analysis of a Δ*pmk1* mutant, PRM of a conditional *pmk1*[AS] mutant and an in vitro kinase assay, we can conclude that Hox7 is phosphorylated at S158 in a Pmk1-dependent manner within a MAP kinase phosphorylation motif (Fig. 5). We have also demonstrated that Pmk1-dependent Hox7 phosphorylation is required for its biological function because a Δ*hox7* mutant cannot be complemented by a non-phosphorylatable Hox7 protein, while expression of a phosphomimetic allele of *HOX7* is
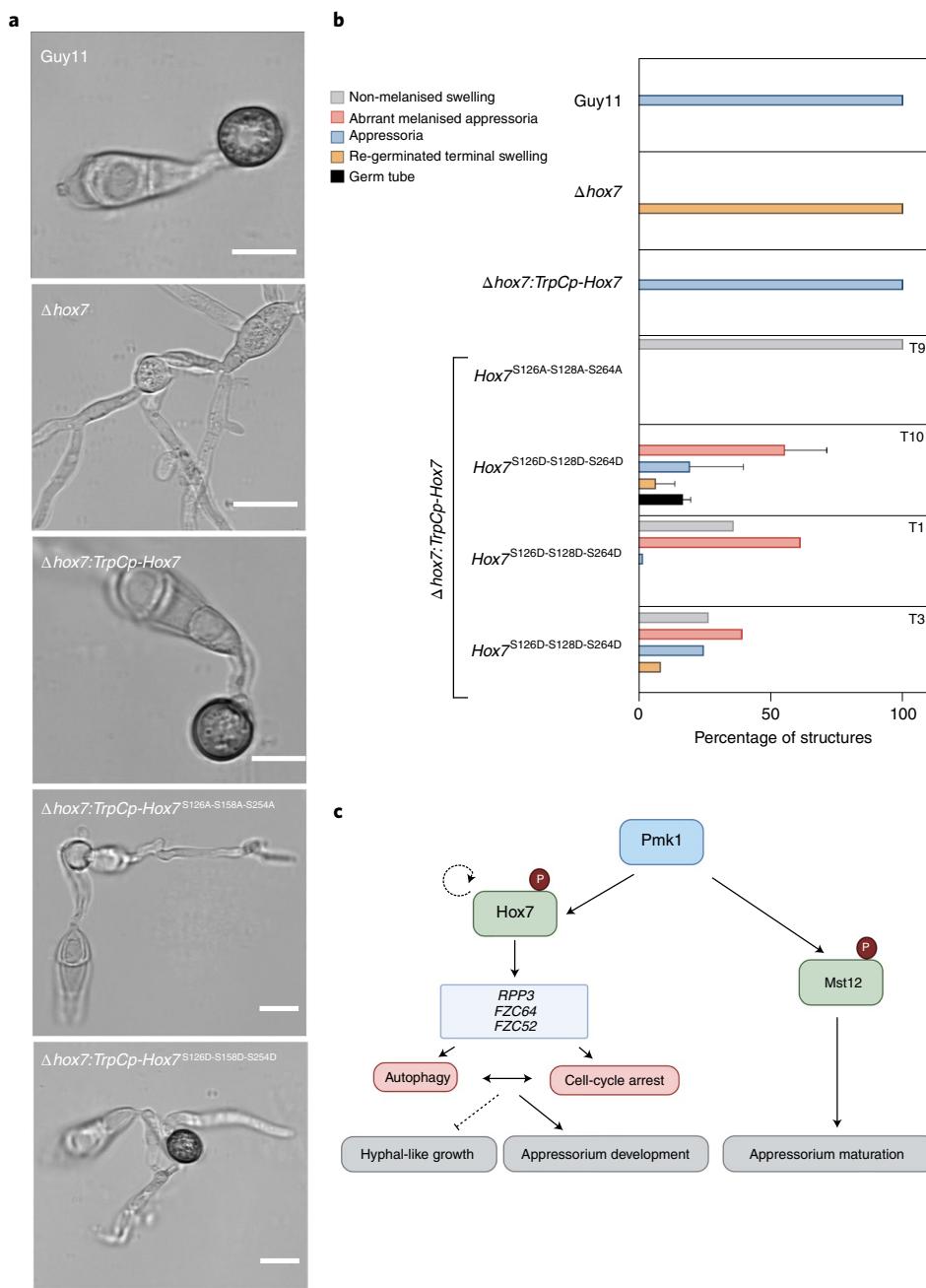
Fig. 7 | Pmk1-dependent phosphorylation of Hox7 is required for appressorium development. a, Micrographs showing appressorium development of Guy11, the Δ*hox7* null mutant, complemented strain Δ*hox7:TrpC-Hox7*, Δ*hox7* null mutant expressing a phospho-dead allele of *Hox7* (Δ*hox7:TrpCp-Hox7*$^{S126A-S158A-S254A}$; Transformant 9, T9) and Δ*hox7* null mutant expressing a phosphomimetic allele of *Hox7* (Δ*hox7:TrpCp-Hox7*$^{S126D-S158D-S254D}$). Micrographs were obtained following conidial incubation on an HP surface for 24 h. Scale bars, 10 μm. Expression of a *Hox7* phosphomimetic allele can restore appressorium formation, whereas the *Hox7* phospho-dead allele fails to complement Δ*hox7*. **b**, Frequency of infection structure formation by Guy11; Δ*hox7*; and the Δ*hox7:TrpC-Hox7*, Δ*hox7:TrpCp-Hox7*$^{S126A-S158A-S254A}$ and Δ*hox7:TrpCp-Hox7*$^{S126D-S158D-S254D}$ transformants (T10, T1 and T3 are three independent fungal transformants from three independent fungal transformation experiments). Three biological replicates of the experiment were performed. A total of 476 structures were counted for the entire experiment; data are the mean ± s.e.m. **c**, Model illustrating hierarchical control of gene expression by the Pmk1 MAPK and associated TFs Hox7 and Mst12 in *M. oryzae*. Hox7 is directly phosphorylated by Pmk1 at S158, which may also exert a positive effect on *HOX7* gene expression (dotted line). Hox7 directly regulates expression of Clade 4–associated TF-encoding genes *RPP3*, *FZC64* and *FZC52*, as well as targets to regulate autophagy and cell cycle arrest following the initial round of mitosis, following conidial germination. Hox7 induces appressorium development and represses hyphal growth. Pmk1 also phosphorylates Mst12 at S133 to regulate the expression of genes associated with maturation of the appressorium, including septin-dependent cytoskeletal re-organization and, re-polarization, exocytosis and effector expression.

sufficient to restore appressorium development. The range of phenotypes observed in mutants expressing a phosphomimetic allele of *HOX7* also provides evidence for the fundamental role of this TF in germ-tube development and appressorium morphogenesis, including a potential inhibitory effect on hyphal growth. As a direct target of Pmk1, Hox7 seems to be positioned at the top of a hierarchy of TFs associated with appressorium morphogenesis, which is consistent with the significant overlap in DEGs of both the Δ*pmk1*

and Δ*hox7* mutants. ChIP–seq furthermore revealed three of the Clade 4 TFs—*FZC64*, *FZC52* (ref. [36]) and *RPP3*—to be targets of Hox7, suggesting that they may constitute the next layer of a hierarchy of transcriptional regulators.

Homeobox TFs act both as activators and repressors of gene expression during multicellular development[47]. They were first described as developmental-switch genes in *Drosophila melanogaster* and subsequently in many other eukaryotes[48,49]. Homeobox TFs have also been extensively studied in cancer biology, where they are implicated in the control of autophagy and cell-cycle regulation. In glioblastomas, for example, HoxC9 acts as a negative regulator of autophagy by controlling activation of beclin1, by regulating transcription of death-associated protein kinase1 (ref. [50]), whereas in neuroblastomas, HoxC9 interacts directly with cyclins to promote G1 arrest by downregulating the transcription of cyclin and CDK genes[51]. Here we have shown how Pmk1 and Hox7 are both essential for the expression of autophagy-related and cell cycle-control genes during appressorium morphogenesis. Hox7 may therefore be essential for G1 arrest in the appressorium nucleus, which follows the initial round of mitosis in the germ tube after conidial germination, given its regulation of genes potentially involved in G1 regulation—such as *Dun1*, *Cds1* and *Chk1*—and the multiple rounds of mitosis observed in the Δ*hox7* mutants[7,25]. This is consistent with Pmk1-dependent phosphorylation of Dun1 and Far1. Cell-cycle arrest may be necessary to repress hyphal-like growth and trigger conidial cell death, but the mechanism by which this occurs and precise interplay with the initiation of autophagy in the conidium require further study. One possibility is that Hox7 is influenced by starvation stress because appressorium development is repressed by exogenous nutrients[1,23,52]. However, the TOR-dependent metabolic checkpoint, reported to lead to a G2 arrest in the conidial nucleus before mitosis[9–11], is not necessary for the action of Pmk1 or Hox7, because TOR inactivation by rapamycin or induction of G2 arrest with benomyl have no effect on the mutant phenotypes of either regulator. How nutrient-sensing affects Hox7 is therefore unclear but interplay with the Snf1 kinase pathway may occur. In yeast[53], Snf1 regulates Atg1 and Atg13, acting antagonistically to the cyclin protein kinase Pho85, which in turn is a negative regulator of autophagy[54]. Moreover, Pho85 regulates infection-associated morphogenesis and virulence in pathogenic fungi such as *Ustilago maydis* and *C. albicans*[55–57]. In *M. oryzae*, Snf1 mutants are impaired in appressorium development, lipid mobilization and turgor generation[58], but the role of Snf1 in the control of autophagy, cell-cycle progression and its relationship to the TOR-dependent metabolic checkpoint[9–11] are unknown. Investigating the interplay of Snf1 and Pho85 with Hox7 may therefore prove valuable in future.

The role of Mst12 is also more clearly defined by this study. Mst12 is directly phosphorylated by Pmk1 at S133 within a MAPK phosphorylation motif but acts in a very distinct way to Hox7, controlling expression of more than 2,000 genes involved in appressorium function. For example, *RVS167*, which is implicated in septin-dependent appressorium re-polarization[15], is a direct target of Mst12. However, Mst12 also regulates an additional 53 TFs as well as genes associated with plant tissue colonization, including a subset of effectors involved in suppression of host immunity. Together, our observations suggest that the Mst12 TF regulates a wide range of functions associated with fungal invasive growth.

In summary, we have provided evidence that Pmk1 MAPK acts as a global regulator of appressorium development and fungal invasive growth by controlling a hierarchical network of transcriptional regulators, including Hox7 and Mst12. In this way appressorium morphogenesis can be seen to be orchestrated by a small number of master regulators acting directly downstream of Pmk1 that are responsible for direct regulation of a set of target genes, including a large family of TF-encoding genes, collectively necessary for the rapid elicitation of the extensive transcriptome changes required for appressorium development.

Methods

Fungal strains, growth conditions and plant infection assays. All of the *M. oryzae* isolates used and generated in this study are stored in the laboratory of N.J.T. (The Sainsbury Laboratory). Fungal strains were routinely incubated at 26 °C with a 12 h photoperiod on complete medium[1]. Rice infections were performed using the blast-susceptible rice (*Oryza sativa*) cultivar CO-39 (ref. [59]). For plant infections, conidial suspensions (5×10^4 conidia ml^{-1} in 0.1% gelatin) were spray-inoculated onto three-week-old seedlings and incubated for 5 d in a controlled-environment chamber at 24 °C with a 12 h photoperiod and 90% relative humidity. The disease-lesion density was recorded 5 d post inoculation, as described previously[60]. Fungal transformations were carried out as previously described[60]. For leaf spot infection experiments, one-week-old leaves of the barley cultivar Golden Promise were spot-inoculated with 20 μl of a 1×10^4 conidia ml^{-1} suspension in 0.2% gelatin in unwounded and needle-wounded leaves. The leaves were incubated on humidity chambers, and lesions were harvested after 5 d and transferred to 2 ml tubes with 300 μl of double-distilled water. Spores from the lesions were recovered by vortex mixing and quantified. The experiments were repeated at least three times.

Generation of GFP fusion plasmids and strains expressing GFP and RFP fusions. The corresponding DNA sequences were retrieved from the *M. oryzae* database (http://fungi.ensembl.org/Magnaporthe_oryzae/Info/Index). In-Fusion cloning (In-Fusion cloning kit, Clontech Laboratories) was used to generate Flp1–GFP and Flp2–GFP. The sequences of the primers used are provided in Supplementary Table 13. Amplified fragments were cloned into HindIII-digested 1284 pNEB-Nat-Yeast vector with the *BAR* gene conferring bialophos (BASTA) resistance. Plasmids expressing GFP and RFP fusions were transformed into Guy11, and Δ*pmk1*, Δ*mst12* and Δ*hox7* mutants and *M. oryzae* transformants with single insertions were selected by Southern blot analysis. Independent *M. oryzae* transformants were used for screening and selected for consistency of fluorescence localization.

Generation of complementation, phosphomimetic and phospho-dead strains. In-Fusion cloning (Clontech Laboratories) was used to generate Mst12–GFP, TrpCp-Hox7, TrpCp-Hox7$^{S126A-S158A-S254A}$, TrpCp-Hox7$^{S126D-S158D-S254D}$ and hox7p:Hox7 (2, 1.5 and 1 kb) using the primers in Supplementary Table 13. Mst12 amplified fragments were cloned into 1284 pNEB-Nat-Yeast cloning vector with the *BAR* gene conferring bialophos (BASTA) resistance. Hox7 fragments were cloned into pCB1532 containing a sulfonylurea-resistant allele of the *ILV2* gene encoding acetolactate synthase under the *A. nidulans* TrpC promoter or Hox7 native promoter. The plasmid constructs were introduced ectopically into fungal strains via PEG-mediated transformation[60]. Presence of the phosphomimetic and phospho-dead alleles was confirmed by Phusion PCR, cleaned enzymatically using ExoSAP-IT PCR product cleanup reagent (Thermo Fisher Scientific) and sequenced. Transformants with single insertions of Mst12–GFP plasmid were confirmed by quantitative PCR by iDna Genetics Ltd.

Generation of *M. oryzae* targeted gene deletion mutants. Targeted gene replacement mutants of *M. oryzae*[60] were generated using the split marker technique[6]. Gene-specific, split marker constructs were amplified using the primers in Supplementary Table 13 and fused with the bialophos (BASTA)-resistance cassette or hygromycin-resistance gene cassette transformed either into Guy11 or Δ*ku70*. Transformants were selected on glufosinate (30 μg ml^{-1}) or hygromycin (200 μg ml^{-1}) and assessed by Southern blot analysis to verify complete deletion of each gene.

In vitro appressorium development assays and live-cell imaging. Appressorium development was induced on borosilicate 18 mm × 18 mm glass coverslips, termed the HP surface in all experiments (Fisher Scientific). Conidial suspensions were prepared at 5×10^4 conidia ml^{-1} in double-distilled water, and 50 μl of the conidial suspension was placed on the coverslip surface and incubated in a controlled-environment chamber at 24 °C. For incubation on non-inductive surfaces, the hydrophilic surface of Gelbond (Sigma) was used (the HL surface). Epifluorescence and differential interference contrast microscopy were carried out using an IX81 motorized inverted microscope (Olympus) and images were captured using a Photometrics CoolSNAP HQ2 camera (Roper Scientific) under control of the MetaMorph v7.8 software (MDS Analytical Technologies). Datasets were compared using an unpaired Student's *t*-test. For the rapamycin exposure experiment, conidia were harvested from nine-day-old cultures and resuspended in 1 μg ml^{-1} rapamycin (Sigma). The spore suspensions were inoculated onto HP coverslips for 24 h. For the benomyl exposure experiment, conidia were harvested from nine-day-old cultures and spore solutions were prepared. Conidial suspensions were prepared at 5×10^4 conidia ml^{-1} in double-distilled water incubated on HP coverslips. At 2.5 h, 50 μM benomyl (Sigma) was added to the conidial suspensions. After 3 h, benomyl was removed with sterile double-distilled water. Images were acquired at 24 h to determine the frequency of appressorium

formation. Solvent-only (dimethylsulfoxide) control experiments were carried out for all drug treatments.

RNA extraction and RNA-seq analysis. For time-series appressorial RNA-seq analysis, conidia were harvested from ten-day-old complete medium agar plates, washed and conidial suspensions (7.5×10^5 conidia ml^{-1}) were prepared in the presence of 50 ng μl^{-1} 1,16-hexadecanediol (Sigma). This spore suspension was poured into square Petri dishes (Greiner Bio One), to which ten glass coverslips (Cole-Parmer) were attached with adhesive. Appressorium formation was monitored using a Will-Wetzlar light inverted microscope (Wilovert, Hund Wetzlar) for each time point, ensuring homogeneous, synchronized infection structure formation. Samples were collected and total RNA was extracted using the Qiagen RNeasy plant mini kit according to manufacturer's instructions. RNA-seq libraries were prepared using 5 μg total RNA with a True-Seq RNA sample preparation kit from Illumina (Agilent) according to the manufacturer's instructions and sequenced using an Illumina 2000 Sequencer. Output short reads were aligned against *M. oryzae* genome sequence version 8.0 using the TopHat software[61]. Data analysis was performed using DESeq, which determines differential gene expression using the mod_lfc value[62]. Transcript abundances for each gene and P_{adj} values were generated. To determine the significant differences of the pairwise comparisons, the P value was adjusted to $P \leq 0.01$.

For mycelial RNA-seq, two-day-old *M. oryzae* mycelium liquid cultures were grown at 24 °C with shaking at 125 r.p.m. Samples were collected and total RNA extracted using RNeasy Plant Mini kit (Qiagen) according to the manufacturer's instructions. Samples were sent to Novogene for library preparation and sequencing using the HiSeq 2500 Illumina technology. Raw reads were aligned to the reference genome 70-15 version 8 transcript FASTA file using a pseudo aligner Kallisto to obtain transcript abundance as transcripts per million[63]. The R package DESeq was used to determine log$_2$-transformed fold change values to identify DEGs. To analyse ChIP–seq results using IGV viewer, raw reads were cleaned and trimmed using fastp v. 0.20.1 and reads were mapped using hisat2 v. 2.1.0. The mapping parameters used were '–dta -t–no-softclip -k 10–score-min L,0,–0.6– reorder–no-unal'. The mapped reads were stored in the BAM format and were sorted and indexed using Samtools v. 1.5.

Protein extraction, phosphoprotein-enrichment, mass-spectrometry analysis for discovery phosphoproteomics, PRM and phosphopeptide quantification. Total protein was extracted from lyophilized *M. oryzae* appressoria from Guy11 and germlings of Δ*pmk1* mutants generated on borosilicate glass coverslips (18 mm × 18 mm; Thermo Fisher Scientific) at 0, 1, 1.5 and 2 h for the PRM experiment. For discovery phosphoproteomics, total protein was extracted from lyophilized *M. oryzae* appressoria from Guy11 and the Δ*pmk1* and Δ*hox7* mutants generated on borosilicate 18 mm × 18 mm glass coverslips (HP; Thermo Fisher Scientific) at 6 h, as performed for the RNA-seq experiments. Lyophilized appressoria were resuspended in extraction buffer (8 M urea, 150 mM NaCl, 100 mM Tris, pH 8, 5 Mm EDTA, 1 μg ml^{-1} aprotinin and 2 μg ml^{-1} leupeptin), mechanically disrupted in a 2010 GenoGrinder tissue homogenizer (1 min at 1,300 r.p.m.) and centrifuged for 10 min at 16,000g at 4 °C (Eppendorf Micro-centrifuge 5418). The supernatant was removed and used to determine the total protein concentration using the Bradford assay. For phosphopeptide enrichment, sample preparation started from 1–3 mg of total protein extract dissolved in ammonium bicarbonate buffer containing 8 M urea. First, the protein extracts were reduced with 5 mM Tris (2-carboxyethyl) phosphine (TCEP) for 30 min at 30 °C with gentle shaking, followed by alkylation of cysteine residues with 40 mM iodoacetamide at room temperature for 1 h. The samples were diluted to a final concentration of 1.6 M urea with 50 mM ammonium bicarbonate and digested overnight with trypsin (Promega; enzyme-to-substrate ratio of 1:100). Peptide digests were purified using C18 SepPak columns (Waters), as described previously[64]. Phosphopeptides were enriched using titanium dioxide (GL Science) with phthalic acid as a modifier[64]. Finally, the phosphopeptides were eluted by a pH shift to 10.5 and immediately purified using C18 microspin columns (The Nest Group Inc.; 5–60 μg loading capacity). After purification, all of the samples were desiccated in a SpeedVac, stored at −80 °C and resuspended in 2% acetonitrile with 0.1% trifluoroacetic acid before mass-spectrometry analysis. LC–MS/MS analysis was performed using an Orbitrap Fusion trihybrid mass spectrometer (Thermo Scientific) and nanoflow ultra-high-performance liquid chromatography (UHPLC) system (Dionex Ultimate3000, Thermo Scientific). Peptides were trapped to a reverse phase trap column (Acclaim PepMap, C18, 5 μm, 100 μm × 2 cm; Thermo Scientific). The peptides were eluted in a gradient of 3–40% acetonitrile in 0.1% formic acid (solvent B) over 120 min, followed by a gradient of 40–80% solvent B over 6 min at a flow rate of 200 nl min^{-1} at 40 °C. The mass spectrometer was operated in positive-ion mode with nano-electrospray ion source with a fused silica emitter with an inner diameter of 0.02 mm (New Objective). A voltage of 2,200 V was applied via platinum wire held in PEEK T-shaped coupling union, with the transfer capillary temperature set to 275 °C. The Orbitrap mass-spectrometry scan resolution of 120,000 at 400 *m/z*, range of 300–1,800 *m/z*, was used, and the automatic gain control was set to 2×10^5 and maximum injection time to 50 ms. In the linear ion trap, MS/MS spectra were triggered using a data-dependent acquisition method, with 'top speed' and 'most intense ion' settings. Selected

precursor ions were fragmented sequentially in both the ion trap using collision-induced dissociation and in the higher-energy collisional dissociation cell. The dynamic exclusion was set to 15 s. The charge state allowed between +2 and +7 charge states to be selected for MS/MS fragmentation.

Peak lists in Mascot generic file format (.mgf files) were prepared from raw data using the MSConvert package (Matrix Science). Peak lists were searched on Mascot server v. 2.4.1 (Matrix Science) against either *M. oryzae* (isolate 70-15, version 8) database or an in-house contaminants database. The MS/MS peak lists were exported using Discoverer v2.2 (Thermo Scientific). Tryptic peptides with up to two possible mis-cleavages and charge states +2, +3 and +4 were allowed in the search. The following modifications were included in the search: oxidized methionine, phosphorylation on serine, threonine, tyrosine as variable modification and carbamidomethylated cysteine as static modification. Data were searched with a monoisotopic precursor and fragment ion mass tolerance of 10 ppm and 0.6 Da, respectively. The Mascot results were combined in Scaffold v. 4 (Proteome Software) to validate the MS/MS-based peptide and protein identifications, and annotate spectra. The position of the modified residue and the quality of spectra for individual phosphopeptides were manually inspected and validated.

Peptide quantitation was performed using PRM, as described previously[65]. The phosphopeptides RLS[+80]FGDDQEER, DNRPLS[+80]PVTLSGGPR and AM[+16]S[+80]GDEYM[+16]M[+16]EQHR were targeted to measure Hox7 phosphorylation at S126, S158 and S254, respectively. The PRM assay also included a selection of control peptides (Supplementary Table 11) with similar relative intensities in each sample and used to measure the relative phosphopeptide content. Target peptide intensities were normalized to the summed control peptide intensities to correct for differences in phosphopeptide yield. The assays were performed for two or three biological replicates with one or two technical replicates and results are provided as the mean ± s.d.

ChIP–seq assays. Two-day-old *M. oryzae* mycelium liquid cultures were grown at 24 °C with shaking at 125 r.p.m. The mycelium (2 g) was cross-linked with 1% formaldehyde for 15 min, followed by a 5 min incubation with 125 mM glycine. The cross-linked mycelium samples were ground to fine powder and resuspended in Honda buffer (20 mM HEPES, 0.44 M sucrose, 1.25% (wt/vol) Ficoll, 2.5% (wt/vol) dextran T40, 10 mM MgCl$_2$, 0.5% Triton X-100, 5 mM dithiothreitol and 1×protease inhibitor mixture (Roche)). The suspension was filtered through sterile Miracloth (Calbiochem), washed twice with sterile distilled water and centrifuged at 3,500g for 5 min. The nuclear pellets were resuspended in four volumes of Nuclei lysis buffer (50 mM Tris–HCl, pH 8.0, 10 mM EDTA, 1% SDS and 1×protease inhibitor mixture) and sonicated with 15 pulses of 30 s (30 s intervals) using a Diagenode Bioruptor (high setting). Immunoprecipitation was carried out overnight at 4 °C using GFP-trap beads (Chromotek) and anti-FLAG M2 beads (Invitrogen). Reverse cross-linking was carried out overnight with 5 M NaCl at 65 °C and 600 r.p.m., followed by treatment with 40 μg proteinase K for 1–2 h at 45 °C. The samples were treated with a ChIP DNA kit concentrator kit (Zymogen) and finally eluted in a volume of 15–20 μl. The samples were sent to BGI Genomics for library preparation and 50 bp single-end sequencing using HiSeq 2500 (Illumina). The reads were mapped, cleaned and aligned to *M. oryzae* genome version 8 using BWA aligner v. 0.5.7. Peaks were identified by MACS2 version 2.1.1 (ref. [66]) with the following parameters: -g 41027733 -q 0.1–bdg— nomodel–extsize 180–broad–broad-cutoff 0.1. Sequences under the peaks were predicted for ±2 kb flanks and analysed using Python bespoke scripts. Motif discovery was carried out using MEME and MEME-ChIP (https://meme-suite. org/meme/index.html). Data visualization was carried out using Integrative Genome Viewer[67]. Motif abundance was tested in ±2 kb regions of DEGs (mod_lfc < −1 or mod_lfc > 1 and P_{adj} < 0.01) of the RNA datasets of mycelium and appressorium development of Δ*hox7* versus Guy11 and Δ*mst12* versus Guy11 using FIMO (https://meme-suite.org/meme/index.html).

Cloning for heterologous protein purification and in vitro kinase phosphorylation assay. For protein expression, complementary DNA encoding full-length Pmk1, full-length Mst12 and Hox7 containing MAPK docking domain and MAPK phosphorylation motif (Met1-Q342) were amplified and cloned into the pOPINM, pOPINS3C and pOPINM vectors, respectively[68], using the In-Fusion cloning technique (Takara Bio) and the primers in Supplementary Table 13. The pOPINM constructs encoding Pmk1, Mst12 and Hox7 fused to the amino-terminal solubility tags 6×His–GST–Pmk1, 6×His–SUMO–Mst12 and 6×His–MBP–Hox7 were transformed into *E. coli* Rosetta (DE3) pLysS. The cells were cultured in LB medium at 37 °C for 6 h, followed by induction with 1 mM isopropyl β-D-1-thiogalactopyranoside at 16 °C overnight. The cells were harvested by centrifugation and resuspended in 50 mM Tris–HCl, pH 7.5, 500 mM NaCl, 50 mM glycine, 5% (vol/vol) glycerol and 20 mM imidazole supplemented with EDTA-free protease inhibitor tablets (cOmplete Roche). The cells were lysed by sonication and the cell debris were removed by centrifugation. The clarified lysate was purified by immobilized metal affinity Natchromatography using a HisTrap column (GE Life Sciences) connected to a Superdex 75 16/60 or Superdex 200 16/60 gel filtration column pre-equilibrated in 20 mM HEPES, pH 7.5 and 150 mM NaCl using an AKTA Xpress purification system (GE Life Sciences). Fractions

containing His-tagged proteins were pooled and concentrated to 1–3 mg ml^{-1}. The purified protein was confirmed by SDS–PAGE analysis and mass spectrometry. Heterologous production and purification of MEK2^{DD} was performed as previously described[46].

For in vitro phosphorylation assays, 6×His–GST-tagged Pmk1 (250 ng) was activated by incubation with recombinant MEK2^{DD} (250 ng). Recombinant 6×His–SUMO-tagged Mst12 (500 ng) and 6×His–MBP-tagged Hox7 (500 ng) were incubated with active Pmk1 in kinase buffer (25 mM Tris, pH 7.5, 10 mM MnCl$_2$, 1 mM EGTA and 1 mM dithiothreitol) in the presence of 1 mM ATP at 30 °C for 30 min. Proteins were separated by SDS–PAGE and transferred to polyvinylidene difluoride membrane using a Trans-Blot turbo transfer system (Bio-Rad). The polyvinylidene difluoride membrane was blocked with 2% BSA in Tris-buffered saline and 1% Tween 20. His-tag detection was carried using polyclonal anti-6×His horseradish peroxidase-conjugated antibody (Abcam). Activated Pmk1 was detected using Phospho-p44/42 MAPK (Erk1/2) (Thr202/Tyr204) (Santa Cruz Biotechnology) and anti-rabbit horseradish peroxidase-conjugated antibodies. Pierce ECL western blotting substrate (Thermo Fisher Scientific) was used for detection. The membranes were imaged using an ImageQuant LAS 4000 luminescent imager (GE Life Sciences). Phosphorylated residues were analysed by LC–MS/MS in data-dependent mode as described earlier.

Statistics and reproducibility. All experiments were conducted with at least two biological replicates and technical replicates of an appropriate sample size, estimated based on what is established in the field. The sample sizes, number of biological and technical replicates, and the statistical tests used in each experiment are specified in the figure legends. No statistical methods were used to pre-determine the sample size and blinding was applied on the disease symptoms of the spray inoculation experiments. For the appressorial development assays, data were analysed using an unpaired two-tailed Student's t-test. $P < 0.05$ was considered significant; *$P < 0.05$, **$P < 0.01$, ***$P < 0.001$ and ****$P < 0.0001$. $P > 0.05$ was considered non-significant and exact values are shown where appropriate. The micrographs where no n is specified in the figure legend represent at least 90 cells over three independent biological replicates. Dot plots were routinely used to show individual data points and generated using Prism7 (GraphPad). Bar graphs of appressorial assays show the mean ± s.e.m. (unless stated otherwise) and were generated using Prism7 (GraphPad). In pathogenicity assays, datasets were tested before comparison for normal distribution using the Shapiro–Wilk normality test. In all cases where at least one dataset was non-normally distributed ($P > 0.05$ in Shapiro–Wilk tests), we used non-parametric Mann–Whitney testing. Analysis of non-normal datasets are represented by box-and-whisker plots that show the 25th and 75th percentiles, the median, and the minimum and maximum values by the ends of the whiskers. A two-tailed Welch's unpaired t-test of three biological replicates with two technical replicates per biological replicate, unless otherwise stated, was applied to the PRM experiments. The DESeq package was used to call differential gene expression (P_{adj}) and the P value was corrected for multiple testing using the Benjamini–Hochberg adjustment. Over-representation of motifs identified by ChIP–seq analysis was verified using the Fisher's exact test.

Reporting Summary. Further information on research design is available in the Nature Research Reporting Summary linked to this article.

Data availability
The RNA-seq data described in this study have been submitted to the European Nucleotide Archive (ENA): appressorial RNA-seq data under the accession number PRJEB36580 and mycelial RNA-seq data under the accession number PRJEB44745. The ChIP–seq data described in this study have been submitted to Gene Expression Omnibus under the accession number GSE182534. The proteomic data described in this study have been deposited into the ProteomeXchange Consortium via PRIDE (Perez-Riverol et al., 2019) partner repository with the dataset identifier PXD025700. The PRM data have been made publicly available through PanoramaWeb (https://panoramaweb.org/84ne1U.url) and the corresponding ProteomeXchange ID for the data is PXD028052. The *M. oryzae* genome database used in this study was http://fungi.ensembl.org/Magnaporthe_oryzae/Info/Index. All *M. oryzae* strains generated in this study are freely available on request from the corresponding authors. Source data are provided with this paper.

Code availability
Scripts for the analysis and prediction of the peaks of ChIP–seq experiments have been publicly deposited in GitHub at https://github.com/threadmapper/sequence-under-peaks.

References
1. Talbot, N. J. On the trail of a cereal killer: exploring the biology of *Magnaporthe grisea*. *Annu. Rev. Microbiol.* **57**, 177–202 (2003).
2. DeZwaan, T. M., Carroll, A. M., Valent, B. & Sweigard, J. A. *Magnaporthe grisea* Pth11p is a novel plasma membrane protein that mediates appressorium differentiation in response to inductive substrate cues. *Plant Cell* **11**, 2013–2030 (1999).
3. Hamer, J. E., Howard, R. J., Chumley, F. G. & Valent, B. A mechanism for surface attachment in spores of a plant pathogenic fungus. *Science* **239**, 288–190 (1988).
4. de Jong, J. C., McCormack, B. J., Smirnoff, N. & Talbot, N. J. Glycerol generates turgor in rice blast. *Nature* **389**, 244–244 (1997).
5. Howard, R. J., Ferrari, M. A., Roach, D. H. & Money, N. P. Penetration of hard substrates by a fungus employing enormous turgor pressures. *Proc. Natl Acad. Sci. USA* **88**, 11281–11284 (1991).
6. Kershaw, M. J. & Talbot, N. J. Genome-wide functional analysis reveals that infection-associated fungal autophagy is necessary for rice blast disease. *Proc. Natl Acad. Sci. USA* **106**, 15967–15972 (2009).
7. Saunders, D. G., Aves, S. J. & Talbot, N. J. Cell cycle-mediated regulation of plant infection by the rice blast fungus. *Plant Cell* **22**, 497–507 (2010).
8. Veneault-Fourrey, C., Barooah, M., Egan, M., Wakley, G. & Talbot, N. J. Autophagic fungal cell death is necessary for infection by the rice blast fungus. *Science* **312**, 580–583 (2006).
9. Marroquin-Guzman, M., Sun, G. & Wilson, R. A. Glucose-ABL1-TOR signaling modulates cell cycle tuning to control terminal appressorial cell differentiation. *PLoS Genet.* **13**, e1006557 (2017).
10. Marroquin-Guzman, M. & Wilson, R. A. GATA-dependent glutaminolysis drives appressorium formation in *Magnaporthe oryzae* by suppressing TOR inhibition of cAMP/PKA signaling. *PLoS Pathog.* **11**, e1004851 (2015).
11. Sun, G., Qi, X. & Wilson, R. A. A feed-forward subnetwork emerging from integrated TOR- and cAMP/PKA-signaling architecture reinforces *Magnaporthe oryzae* appressorium morphogenesis. *Mol. Plant Microbe Interact.* **32**, 593–607 (2019).
12. Ryder, L. S. et al. NADPH oxidases regulate septin-mediated cytoskeletal remodeling during plant infection by the rice blast fungus. *Proc. Natl Acad. Sci. USA* **110**, 3179–3184 (2013).
13. Dagdas, Y. F. et al. Septin-mediated plant cell invasion by the rice blast fungus, *Magnaporthe oryzae*. *Science* **336**, 1590–1595 (2012).
14. Rocha, R. O., Elowsky, C., Pham, N. T. T. & Wilson, R. A. Spermine-mediated tight sealing of the *Magnaporthe oryzae* appressorial pore-rice leaf surface interface. *Nat. Microbiol.* **5**, 1472–1480 (2020).
15. Sakulkoo, W. et al. A single fungal MAP kinase controls plant cell-to-cell invasion by the rice blast fungus. *Science* **359**, 1399–1403 (2018).
16. Giraldo, M. C. et al. Two distinct secretion systems facilitate tissue invasion by the rice blast fungus *Magnaporthe oryzae*. *Nat. Commun.* **4**, 1996 (2013).
17. Xu, J. R. & Hamer, J. E. MAP kinase and cAMP signaling regulate infection structure formation and pathogenic growth in the rice blast fungus *Magnaporthe grisea*. *Genes Dev.* **10**, 2696–2706 (1996).
18. Saunders, D. G., Dagdas, Y. F. & Talbot, N. J. Spatial uncoupling of mitosis and cytokinesis during appressorium-mediated plant infection by the rice blast fungus *Magnaporthe oryzae*. *Plant Cell* **22**, 2417–2428 (2010).
19. Dean, R. A. et al. The genome sequence of the rice blast fungus *Magnaporthe grisea*. *Nature* **434**, 980–986 (2005).
20. Thines, E., Weber, R. W. & Talbot, N. J. MAP kinase and protein kinase A-dependent mobilization of triacylglycerol and glycogen during appressorium turgor generation by *Magnaporthe grisea*. *Plant Cell* **12**, 1703–1718 (2000).
21. Becker, J., Liermann, J. C., Opatz, T., Anke, H. & Thines, E. GKK1032A$_2$, a secondary metabolite from *Penicillium* sp. IBWF-029-96, inhibits conidial germination in the rice blast fungus *Magnaporthe oryzae*. *J. Antibiot.* **65**, 99–102 (2012).
22. Park, G., Xue, C., Zheng, L., Lam, S. & Xu, J. R. MST12 regulates infectious growth but not appressorium formation in the rice blast fungus *Magnaporthe grisea*. *Mol. Plant Microbe Interact.* **15**, 183–192 (2002).
23. Soanes, D. M., Chakrabarti, A., Paszkiewicz, K. H., Dawe, A. L. & Talbot, N. J. Genome-wide transcriptional profiling of appressorium development by the rice blast fungus *Magnaporthe oryzae*. *PLoS Pathog.* **8**, e1002514 (2012).
24. Oses-Ruiz, M. & Talbot, N. J. Cell cycle-dependent regulation of plant infection by the rice blast fungus Magnaporthe oryzae. *Commun. Integr. Biol.* **10**, e1372067 (2017).
25. Oses-Ruiz, M., Sakulkoo, W., Littlejohn, G. R., Martin-Urdiroz, M. & Talbot, N. J. Two independent S-phase checkpoints regulate appressorium-mediated plant infection by the rice blast fungus *Magnaporthe oryzae*. *Proc. Natl Acad. Sci. USA* **114**, E237–E244 (2017).
26. Kulkarni, R. D., Thon, M. R., Pan, H. & Dean, R. A. Novel G-protein-coupled receptor-like proteins in the plant pathogenic fungus *Magnaporthe grisea*. *Genome Biol.* **6**, R24 (2005).
27. Chumley, F. G. & Valent, B. Genetic analysis of melanin deficient, nonpathogenic mutants of *Magnaporthe grisea*. *Mol. Plant Microbe Interact.* **3**, 135–143 (1990).

28. Skamnioti, P. & Gurr, S. J. *Magnaporthe grisea* Cutinase2 mediates appressorium differentiation and host penetration and is required for full virulence. *Plant Cell* **19**, 2674–2689 (2007).

29. Johnson, K. L., Jones, B. J., Bacic, A. & Schultz, C. J. The fasciclin-like arabinogalactan proteins of *Arabidopsis*. A multigene family of putative cell adhesion molecules. *Plant Physiol.* **133**, 1911–1925 (2003).

30. Seifert, G. J. Fascinating fasciclins: A surprisingly widespread family of proteins that mediate interactions between the cell exterior and the cell surface. *Int. J. Mol. Sci.* https://doi.org/10.3390/ijms19061628 (2018).

31. Dong, B. et al. MgAtg9 trafficking in *Magnaporthe oryzae*. *Autophagy* **5**, 946–953 (2009).

32. Petersen, T. N., Brunak, S., von Heijne, G. & Nielsen, H. SignalP 4.0: discriminating signal peptides from transmembrane regions. *Nat. Methods* **8**, 785–786 (2011).

33. Haijiao, L. et al. A novel *Magnaporthe oryzae* gene *MCG1*, encoding an extracellular globular protein, affects conidial germination and appressorial formation. *Int. J. Agric. Technol.* **7**, 1647–1660 (2011).

34. Skamnioti, P., Henderson, C., Zhang, Z., Robinson, Z. & Gurr, S. J. A novel role for catalase B in the maintenance of fungal cell-wall integrity during host invasion in the rice blast fungus *Magnaporthe grisea*. *Mol. Plant Microbe Interact.* **20**, 568–580 (2007).

35. Mosquera, G., Giraldo, M. C., Khang, C. H., Coughlan, S. & Valent, B. Interaction transcriptome analysis identifies *Magnaporthe oryzae* BAS1-4 as biotrophy-associated secreted proteins in rice blast disease. *Plant Cell* **21**, 1273–1290 (2009).

36. Lu, J., Cao, H., Zhang, L., Huang, P. & Lin, F. Systematic analysis of Zn2Cys6 transcription factors required for development and pathogenicity by high-throughput gene knockout in the rice blast fungus. *PLoS Pathog.* **10**, e1004432 (2014).

37. Sweigard, J. A., Carroll, A. M., Farrall, L., Chumley, F. G. & Valent, B. *Magnaporthe grisea* pathogenicity genes obtained through insertional mutagenesis. *Mol. Plant Microbe Interact.* **11**, 404–412 (1998).

38. Felenbok, B. The ethanol utilization regulon of *Aspergillus nidulans*: the alcA–alcR system as a tool for the expression of recombinant proteins. *J. Biotechnol.* **17**, 11–17 (1991).

39. Kim, S. et al. Homeobox transcription factors are required for conidiation and appressorium development in the rice blast fungus *Magnaporthe oryzae*. *PLoS Genet.* **5**, e1000757 (2009).

40. Howard, R. J. & Valent, B. Breaking and entering: host penetration by the fungal rice blast pathogen *Magnaporthe grisea*. *Annu. Rev. Microbiol.* **50**, 491–512 (1996).

41. Kwon, S. et al. Role of the histone acetyltransferase Rtt109 in development and pathogenicity of the rice blast fungus. *Mol. Plant Microbe Interact.* **31**, 1200–1210 (2018).

42. Lane, S., Zhou, S., Pan, T., Dai, Q. & Liu, H. The basic helix-loop-helix transcription factor Cph2 regulates hyphal development in *Candida albicans* partly via Tec1. *Mol. Cell. Biol.* **21**, 6418–6428 (2001).

43. McLeod, M. et al. Cpc2, a fission yeast homologue of mammalian RACK1 protein, interacts with Ran1 (Pat1) kinase to regulate cell cycle progression and meiotic development. *Mol. Cell. Biol.* **20**, 4016–4027 (2000).

44. Mitchell, T. K. & Dean, R. A. The cAMP-dependent protein kinase catalytic subunit is required for appressorium formation and pathogenesis by the rice blast pathogen *Magnaporthe grisea*. *Plant Cell* **7**, 1869–1878 (1995).

45. Xu, J.-R., Urban, M., Sweigard, J. A. & Hamer, J. E. The *CPKA* gene of *Magnaporthe grisea* is essential for appressorial penetration. *Mol. Plant Microbe Interact.* **10**, 187–194 (1997).

46. Menke, F. L. et al. Tobacco transcription factor WRKY1 is phosphorylated by the MAP kinase SIPK and mediates HR-like cell death in tobacco. *Mol. Plant Microbe Interact.* **18**, 1027–1034 (2005).

47. Pearson, J. C., Lemons, D. & McGinnis, W. Modulating Hox gene functions during animal body patterning. *Nat. Rev. Genet.* **6**, 893–904 (2005).

48. McGinnis, W., Garber, R. L., Wirz, J., Kuroiwa, A. & Gehring, W. J. A homologous protein-coding sequence in *Drosophila* homeotic genes and its conservation in other metazoans. *Cell* **37**, 403–408 (1984).

49. Bürglin, T. R. & Affolter, M. Homeodomain proteins: an update. *Chromosoma* **125**, 497–521 (2016).

50. Xuan, F. et al. Homeobox C9 suppresses Beclin1-mediated autophagy in glioblastoma by directly inhibiting the transcription of death-associated protein kinase 1. *Neuro Oncol.* **18**, 819–829 (2016).

51. Mao, L. et al. HOXC9 links cell-cycle exit and neuronal differentiation and is a prognostic marker in neuroblastoma. *Cancer Res.* **71**, 4314–4324 (2011).

52. Wilson, R. A., Gibson, R. P., Quispe, C. F., Littlechild, J. A. & Talbot, N. J. An NADPH-dependent genetic switch regulates plant infection by the rice blast fungus. *Proc. Natl Acad. Sci. USA* **107**, 21902–21907 (2010).

53. Celenza, J. L. & Carlson, M. Mutational analysis of the *Saccharomyces cerevisiae* SNF1 protein kinase and evidence for functional interaction with the SNF4 protein. *Mol. Cell. Biol.* **9**, 5034–5044 (1989).

54. Wang, Z., Wilson, W. A., Fujino, M. A. & Roach, P. J. Antagonistic controls of autophagy and glycogen accumulation by Snf1p, the yeast homolog of AMP-activated protein kinase, and the cyclin-dependent kinase Pho85p. *Mol. Cell. Biol.* **21**, 5742–5752 (2001).

55. Castillo-Lluva, S., Alvarez-Tabarés, I., Weber, I., Steinberg, G. & Pérez-Martin, J. Sustained cell polarity and virulence in the phytopathogenic fungus *Ustilago maydis* depends on an essential cyclin-dependent kinase from the Cdk5/Pho85 family. *J. Cell Sci.* **120**, 1584–1595 (2007).

56. Huang, D., Friesen, H. & Andrews, B. Pho85, a multifunctional cyclin-dependent protein kinase in budding yeast. *Mol. Microbiol.* **66**, 303–314 (2007).

57. Shapiro, R. S. et al. Pho85, Pcl1, and Hms1 signaling governs *Candida albicans* morphogenesis induced by high temperature or Hsp90 compromise. *Curr. Biol.* **22**, 461–470 (2012).

58. Zeng, X.-Q. et al. Crosstalk between SNF1 pathway and the peroxisome-mediated lipid metabolism in *Magnaporthe oryzae*. *PLoS ONE* **9**, e103124 (2014).

59. Valent, B. & Chumley, F. G. Molecular genetic analysis of the rice blast fungus, *Magnaporthe grisea*. *Annu. Rev. Phytopathol.* **29**, 443–467 (1991).

60. Talbot, N. J., Ebbole, D. J. & Hamer, J. E. Identification and characterization of *MPG1*, a gene involved in pathogenicity from the rice blast fungus *Magnaporthe grisea*. *Plant Cell* **5**, 1575–1590 (1993).

61. Trapnell, C. et al. Transcript assembly and quantification by RNA-Seq reveals unannotated transcripts and isoform switching during cell differentiation. *Nat. Biotechnol.* **28**, 511–515 (2010).

62. Anders, S. & Huber, W. Differential expression analysis for sequence count data. *Genome Biol.* **11**, 106 (2010).

63. Bray, N. L., Pimentel, H., Melsted, P. & Pachter, L. Near-optimal probabilistic RNA-seq quantification. *Nat. Biotechnol.* **34**, 525–527 (2016).

64. Mithoe, S. C. et al. Attenuation of pattern recognition receptor signaling is mediated by a MAP kinase kinase kinase. *EMBO Rep.* **17**, 441–454 (2016).

65. Guo, H. et al. Phosphorylation-regulated activation of the *Arabidopsis* RRS1-R/RPS4 immune receptor complex reveals two distinct effector recognition mechanisms. *Cell Host Microbe* **27**, 769–781.

66. Zhang, Y. et al. Model-based analysis of ChIP-Seq (MACS). *Genome Biol.* **9**, R137 (2008).

67. Robinson, J. T. et al. Integrative genomics viewer. *Nat. Biotechnol.* **29**, 24–26 (2011).

68. Berrow, N. S. et al. A versatile ligation-independent cloning method suitable for high-throughput expression screening applications. *Nucleic Acids Res.* **35**, e45 (2007).

69. Turra, D., Segorbe, D. & Di Pietro, A. Protein kinases in plant-pathogenic fungi: conserved regulators of infection. *Annu. Rev. Phytopathol.* **52**, 267–288 (2014).

70. Zhao, X. & Xu, J. R. A highly conserved MAPK-docking site in Mst7 is essential for Pmk1 activation in *Magnaporthe grisea*. *Mol. Microbiol.* **63**, 881–894 (2007).

Acknowledgements

Author contributions

M.O.-R. and N.J.T. conceptualized the project. Experimental analyses were carried out by M.O.-R., N.C-M., M.M.-U., A.B.E., M.N., I.E., X.Y., M.J.K., X.Y., C.M. and G.R.L. F.L.H.M designed, and P.D. and F.L.H.M. carried out, the phosphoproteomic analysis. G.V.-P. and B.V. generated the Δrpp3 mutant. Bioinformatic analysis was performed by M.O.-R., D.M.S., B.T., J.C. and V.W. The paper was written by M.O.-R. and N.J.T., with contributions from all authors.

Competing interests

The authors declare no competing interests.

Additional information
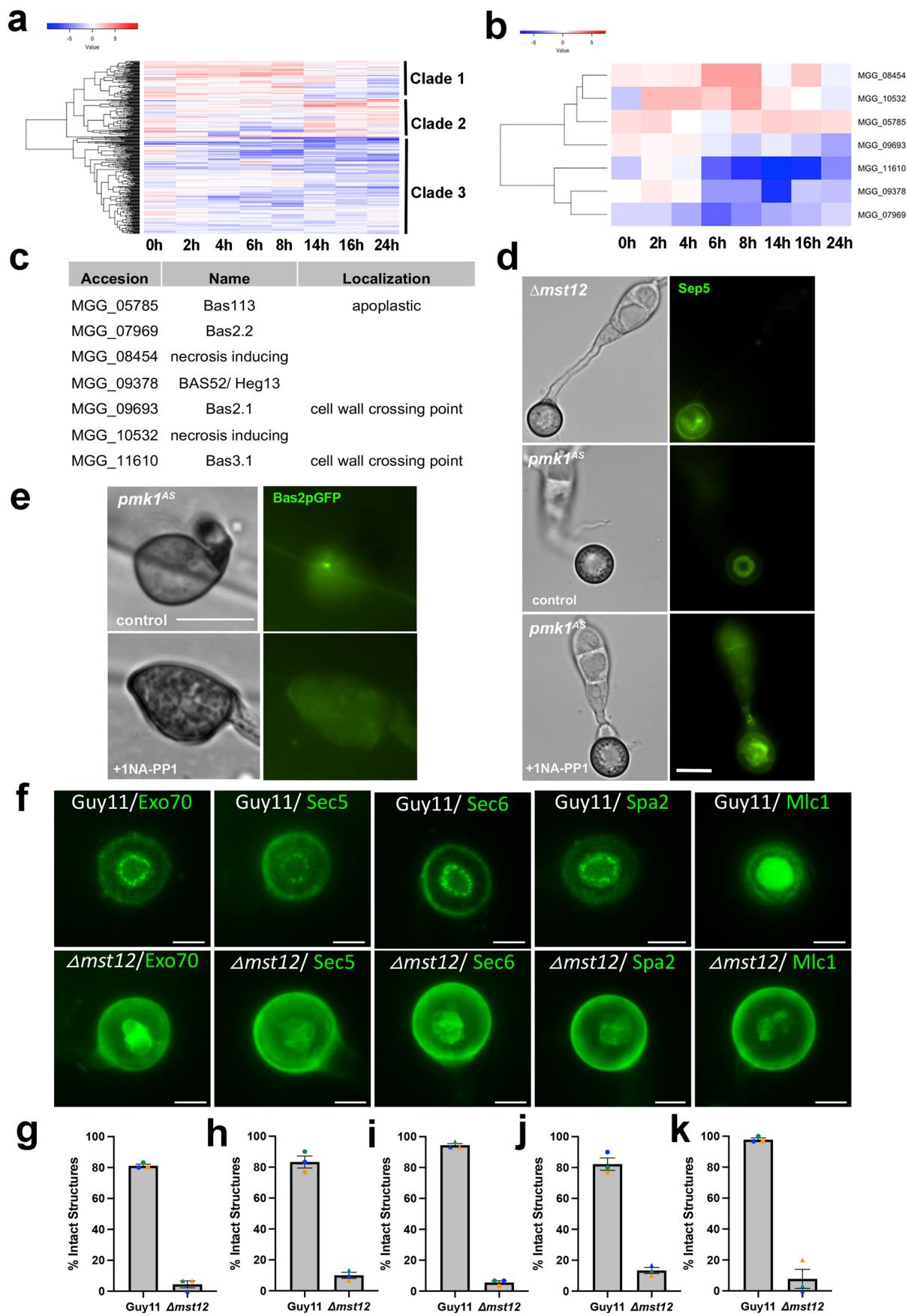
a

b

c

d

Extended Data Fig. 1 | See next page for caption.

Extended Data Fig. 1 | The Pmk1 MAP kinase signalling pathway regulates appressorium development in response to surface hydrophobicity.
a. Micrographs to show development of a wild type *M. oryzae* strain Guy11 expressing histone H1–RFP nuclear marker and septin Sep3–GFP, inoculated on a hydrophobic (HP) or hydrophilic (HL) surface (Scale bar = 10 μm). **b**. Bar chart to show proportion of Guy11 germlings containing, 1, 2, 3, 4 or more nuclei following incubation for 24 h on HP or HL surfaces. (Grey: HP; White: HL; Circles represent replicates for HP surface; Triangles represent replicates for HL surface) (n = 135 conidia examined in 3 biological replicates; each biological replicate is colour coded; data is presented as Mean ±SEM; Multiple unpaired t-test; HP versus HL; 1 nucleus P = 0.014037). **c**. Live-cell imaging to show nuclear number and the presence/absence of conidial autophagic cell death of Guy11 on HP, Δ*pmk1* mutant on HP, and Guy11 on HL surfaces respectively. Each strain expressed the H1–RFP nuclear marker. **d**. Rice blast disease symptoms of Guy11 and the Δ*pmk1* mutant. Rice seedlings of cultivar CO-39 were spray-inoculated with *M. oryzae* conidial suspensions of equal concentrations and incubated for 5 days.

a. Guy11 / Δmst12

b. Guy11 / Δmst12

c.

Gene Name	# Accession
Acetyl-CoA carboxylase	MGG_07613
Polyketide synthase (*ALB1*)	MGG_07219
Tetrahydroxynaphthalene reductase (*4HNR*)	MGG_07216
Scytalone dehydratase (*RSY1*)	MGG_05059
Trihydroxynaphthalene reductase (*BUF1*)	MGG_02252
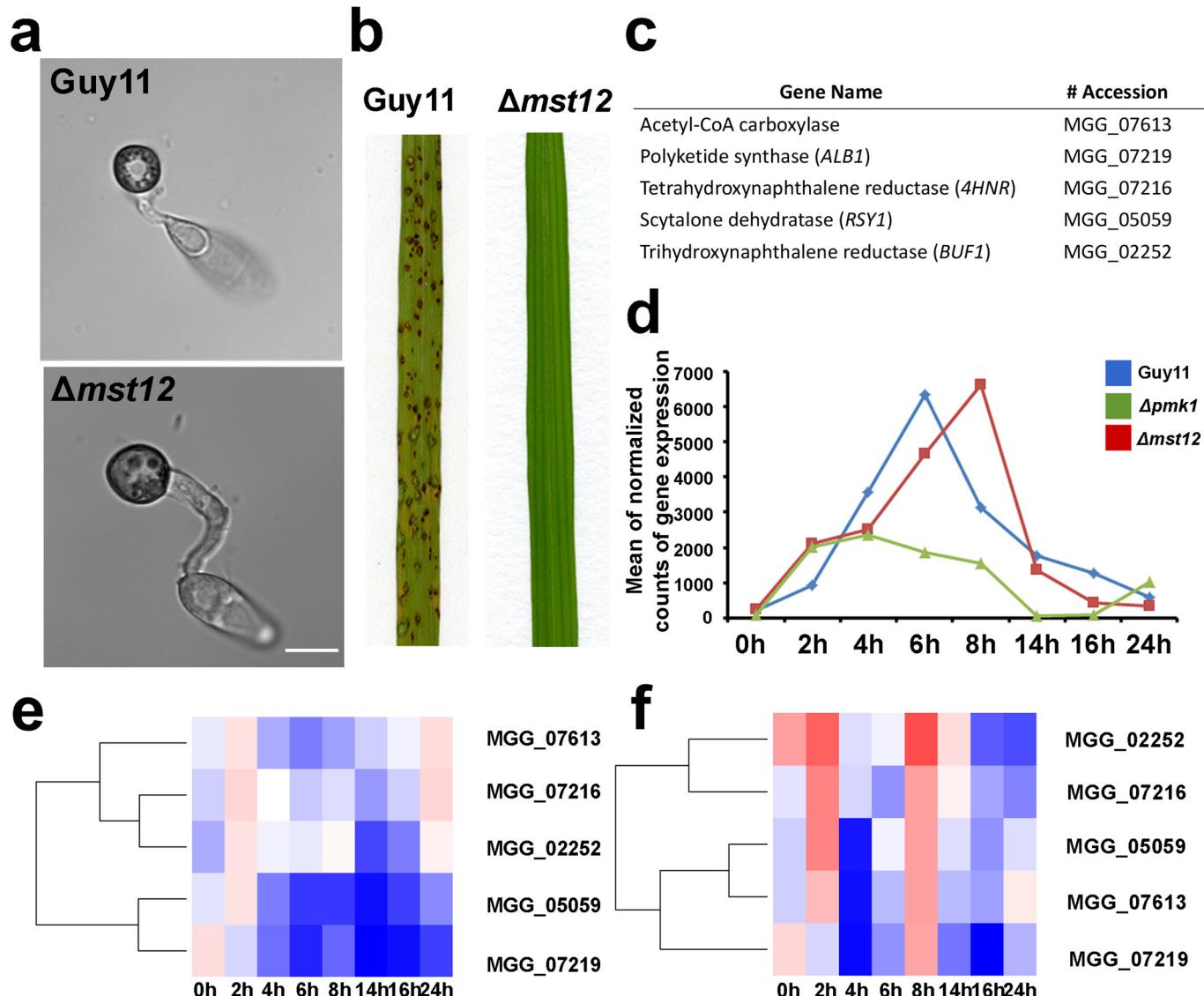
Extended Data Fig. 2 | Expression of melanin biosynthesis pathway genes during appressorium development by *M. oryzae*. a. Micrograph to show appressorium development by Guy11 and Δ*mst12* mutant after incubation for 24 h on HP surface (Bar = 10 μm). **b**. Rice blast disease symptoms caused by Guy11 and Δ*mst12* mutant. Rice seedlings of cultivar CO-39 were spray-inoculated with *M. oryzae* conidial suspensions of equal concentrations and incubated for 5 days. **c**. Table to show names and accession numbers of melanin biosynthesis enzymes of *M. oryzae*. **d**. Line graph to show mean of normalized counts of gene expression of melanin biosynthesis enzyme-encoding genes during a time course appressorium development for Guy11, Δ*pmk1* and Δ*mst12* mutants incubated on HP surface between 0 h and 24 h. **e**. Heatmap to show levels of transcript abundance of genes involved in melanin biosynthesis in a Δ*pmk1* mutant compared to Guy11 in conidia germinated on HP surfaces between 0 h and 24 h. **f**. Heatmap to show levels of transcript abundance of genes involved in melanin biosynthesis in a Δ*mst12* mutant compared to Guy11 incubated on HP surface between 0 h and 24 h. Levels of expression are represented as moderated logarithmic fold change (mod_lfc) (blue= downregulated in mutants versus Guy11; red= upregulated in mutants versus Guy11).

a

Clade 1

Clade 2

Clade 3

0h 2h 4h 6h 8h 14h 16h 24h

b

MGG_08454
MGG_10532
MGG_05785
MGG_09693
MGG_11610
MGG_09378
MGG_07969

0h 2h 4h 6h 8h 14h 16h 24h

c

Accesion	Name	Localization
MGG_05785	Bas113	apoplastic
MGG_07969	Bas2.2	
MGG_08454	necrosis inducing	
MGG_09378	BAS52/ Heg13	
MGG_09693	Bas2.1	cell wall crossing point
MGG_10532	necrosis inducing	
MGG_11610	Bas3.1	cell wall crossing point

d Δmst12 Sep5 / pmk1^AS control / pmk1^AS +1NA-PP1

e pmk1^AS Bas2pGFP control / +1NA-PP1

f Guy11/Exo70 | Guy11/ Sec5 | Guy11/ Sec6 | Guy11/ Spa2 | Guy11/ Mlc1

Δmst12/Exo70 | Δmst12/ Sec5 | Δmst12/ Sec6 | Δmst12/ Spa2 | Δmst12/ Mlc1

g % Intact Structures — Guy11 / Δmst12

h % Intact Structures — Guy11 / Δmst12

i % Intact Structures — Guy11 / Δmst12

j % Intact Structures — Guy11 / Δmst12

k % Intact Structures — Guy11 / Δmst12

Extended Data Fig. 3 | See next page for caption.

Extended Data Fig. 3 | Mst12-dependent gene expression and sub-cellular localization of a subset of *M. oryzae* effectors during appressorium development. a. Heatmap showing temporal pattern of transcript abundance of 436 Mst12-dependent genes predicted to encode secreted proteins during appressorium development between 0 h and 24 h on a HP surface. **b**. Heatmap showing levels of transcript abundance of 7 known effector-encoding genes[2] in a Δ*mst12* mutant during appressorium development. (blue= downregulated in Δ*mst12* mutant versus Guy11; red= upregulated in Δ*mst12* mutant versus Guy11). Levels of expression are represented as moderated logarithmic fold change (mod_lfc) **c**. Table to show name and accession number of 7 known effector genes differentially regulated in Δ*mst12* compared to Guy11. **d**. Live-cell imaging of Septin5-GFP expression in appressoria of Δ*mst12* and *pmk1*[as] mutants 24 h after conidial germination on a HP surface. The *pmk1*[AS] mutant was incubated ± 5 μM NA-PP1 added at 6-8 h, once appressorium development was underway. 1NA-PP1 is a specific inhibitor of the analogue-sensitive allele Pmk1 expressed by this mutant[3] (Bar = 10 μm). **e**. Micrographs to show expression of effector Bas2pGFP in a *pmk1*[AS] mutant during appressorium formation, 24 h after conidia were inoculated on rice leaf sheath of blast-susceptible rice cultivar Mokoto, in the presence or absence (control) of 5 μM 1Na-PP1 (Bar = 10 μm). **f**. Micrographs to show cellular localization of exocyst and polarity proteins Exo70-GFP, Sec5-GFP, Sec6-GFP, Spa2-GFP and Mlc1-GFP in the appressorium pore of Guy11 and Δ*mst12* following incubation on HP surface for 24 h (Bar = 5 μm). **(g-k)**. Bar charts to show defects in localization of exocyst components during appressorium development of Δ*mst12* compared to Guy11 on HP surface at 24 h (n = 180 conidia examined in 3 biological replicates; each biological replicate is colour coded; data are presented as Mean ±SEM).

c
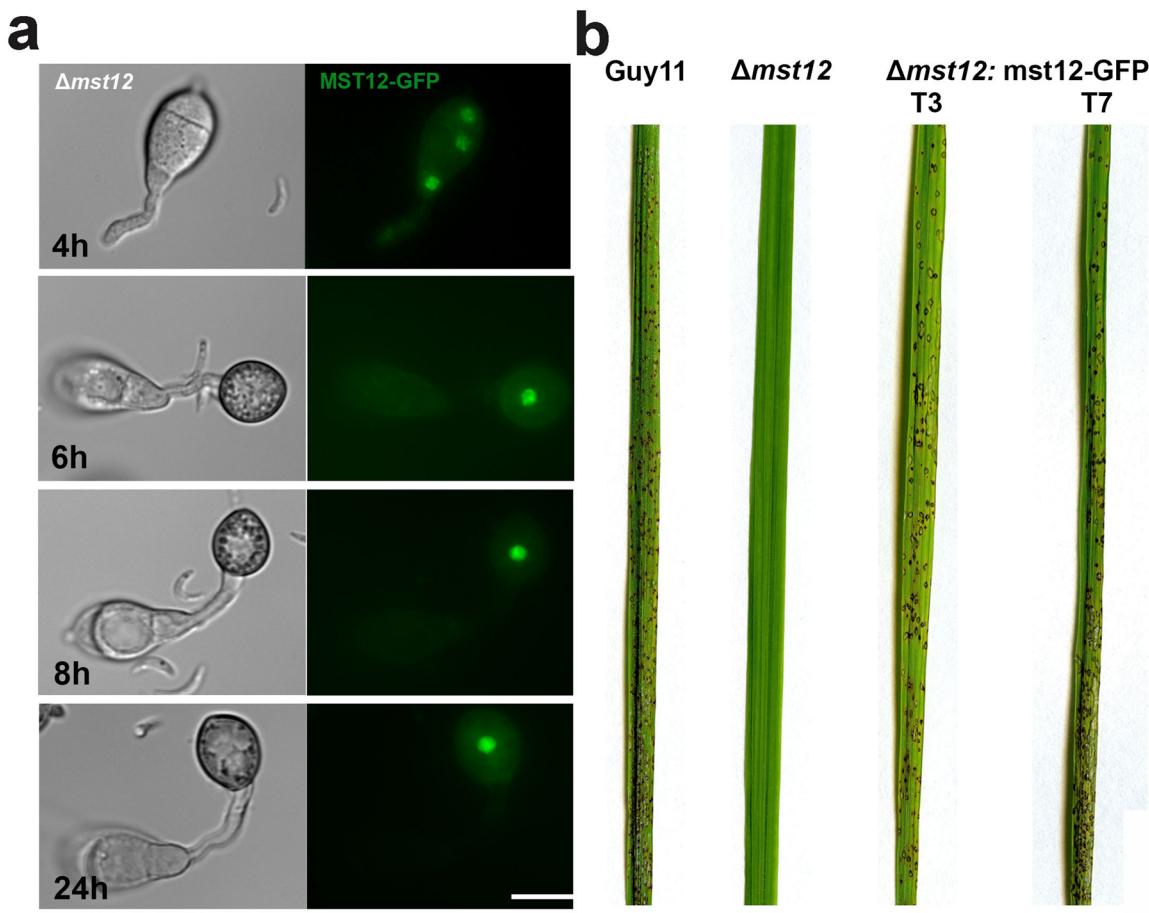
RNA-seq Mycelium	Up mlfc>1	Down mlfc<-1	Total
Δmst12 vs. Guy11	2334	1848	4182

d

Dataset	Motif1	Motif2	Motif3	Total DEGs
	1.9e-221	1.4e-154	1.7e-127	
Whole Genome	3425	2061	2537	
Down Mycelium	609 P = 6.54e^{-111} (32.95%)	328 P = 3.48e^{-44} (17.74%)	430 P = 1.35e^{-67} (23.27%)	1848
Up Mycelium	554 P = 1.28e^{-44} (23.74%)	295 P = 3.33e^{-15} (12.64%)	367 P = 1.25e^{-19} (15.72%)	2334
DEGs Appressorium	670 P = 1.76e^{-76} (26.67%)	376 P = 1.28e^{-33} (14.97%)	420 P = 5.07e^{-28} (16.72%)	2512

Extended Data Fig. 4 | See next page for caption.

Extended Data Fig. 4 | ChIP–seq analysis of the Mst12 TF. a. Micrographs to show cellular localization of Mst12–GFP during appressorium development following incubation on HP surface for 24 h (Bar = 10 μm)**. b**. Rice blast disease symptoms of Guy11, Δ*mst12* mutant and complemented strain Δ*mst12*: Mst12–GFP (T3 and T7 are two independent transformants). Rice seedlings of cultivar CO-39 were spray-inoculated with conidial suspensions of equal concentrations of each *M. oryzae* strain and incubated for 5 days. **c**. Table to show number of differentially regulated genes (p$_{adj}$ <0.01, mod_lfc>1 or mod_lfc < -1) Guy11 and the Δ*mst12* mutant during mycelium growth determined by RNA-seq analysis. **d**. Table to show over-represented motifs in peaks determined in Mst12 ChIP–seq experiment by Find Individual Motif Occurrence (FIMO – see https://meme-suite.org/meme/doc/fimo.html). Over-representation of each motif in specific sets of DEGs (up and downregulated in mycelium, or expressed during appressorium formation) was analysed using Fisher's exact test and *P* values are indicated. The percentage value represents the proportion of the total pool of DEGs represented by that each set of motif-defined gene sets.
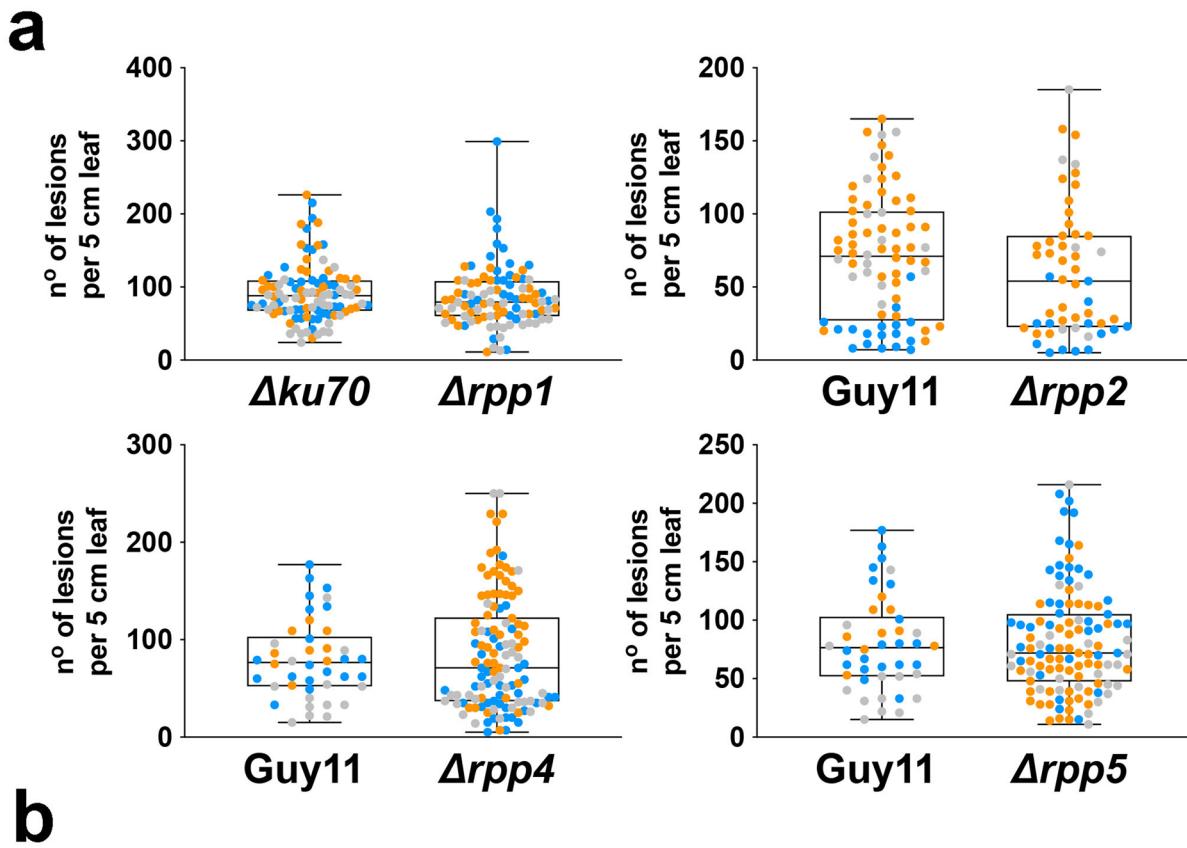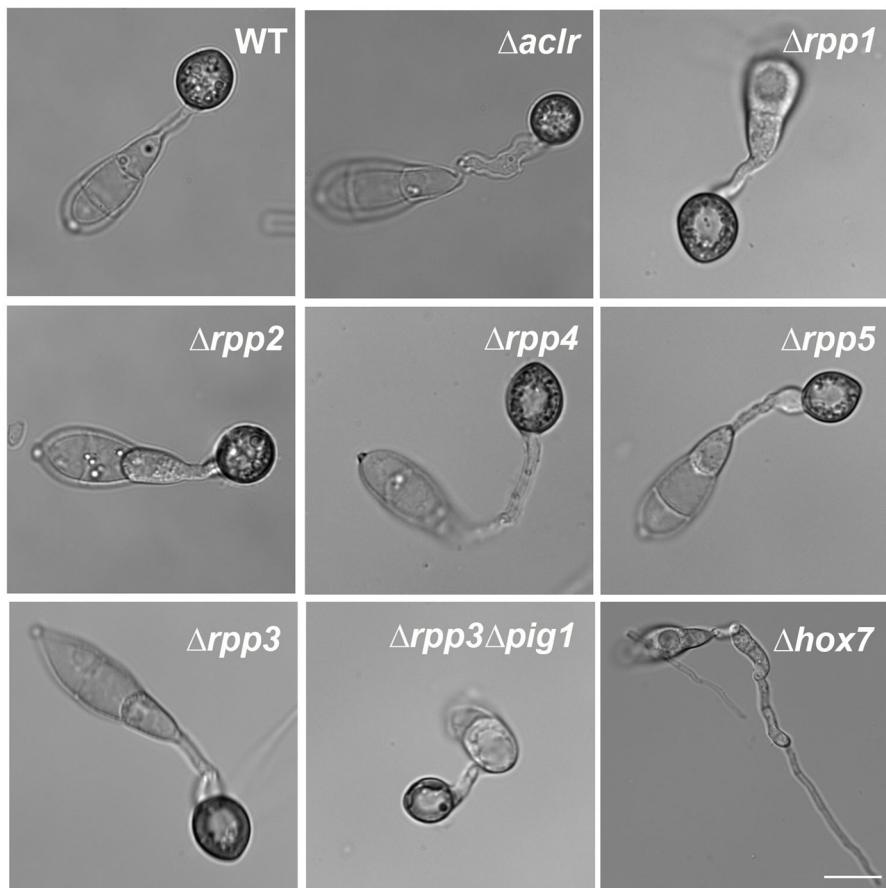
Extended Data Fig. 5 | See next page for caption.

Extended Data Fig. 5 | Appressorium development and pathogenicity assay of clade 4-associated TF null mutants. a. Box and Whisker plots to show the number of rice blast disease lesions per 5 m of leaf tissue. Twenty-one-day-old rice seedlings of rice cultivar Co-39 were inoculated with uniform conidial suspensions (5×10^4 conidia ml^{-1}) of Δ*rpp1*, Δ*rpp2*, Δ*rpp4* and Δ*rpp5* mutants and the isogenic wild type *M. oryzae* strain Guy11 or Δ*ku70*. Data points are shown in whisker plots which show 25th/75th percentiles, the median and the minimum and maximum values by the ends of the whiskers. A two-tailed non-parametric Mann–Whitney statistical test was conducted to determine significant differences. The plots show the results from 3 biological replications of the experiment and data points are colour coded for each replicate. Error bars show the standard deviation. **b**. Light micrographs showing appressorium development of Guy11, Δ*aclR*, Δ*rpp1*, Δ*rpp2*, Δ*rpp4*, Δ*rpp5*, Δ*rpp3*, Δ*rpp3*Δ*pig1* and Δ*hox7* mutants germinated on HP surfaces and observed 24 h following conidial germination (Bar = 10 μm).

b

| 14h	Up mlfc>1	Down mlfc<-1	Total
Δpmk1	1636	2591	4227
Δmst12	632	866	1498
Δhox7	1879	2332	4211
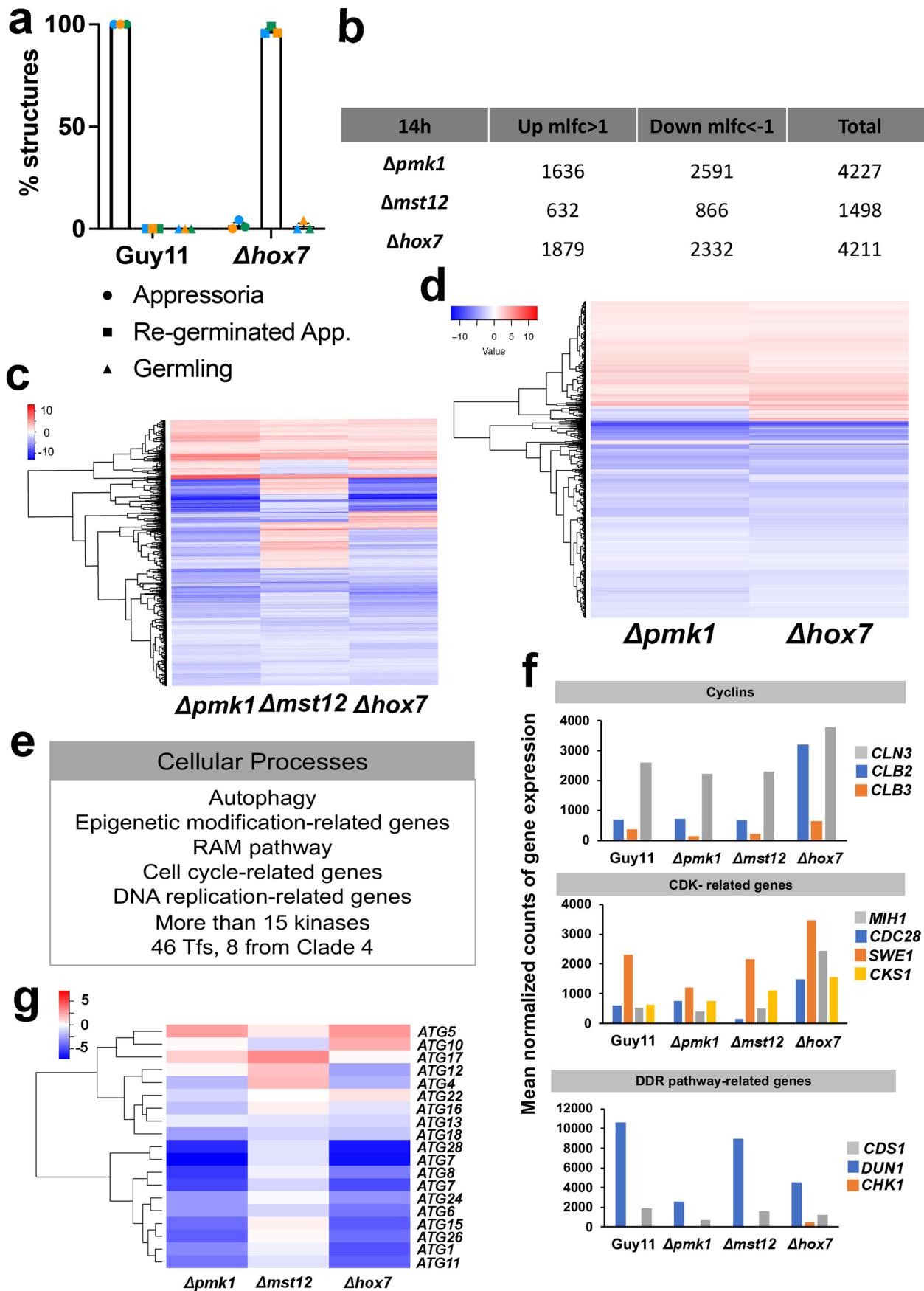
Extended Data Fig. 6 | See next page for caption.

Extended Data Fig. 6 | Hox7 operates downstream of Pmk1 MAP kinase to regulate a subset of cellular pathways required for appressorium development and plant infection. a. Bar chart to show the proportion of germlings of Guy11 and Δ*hox7* that develop appressoria (round data points), re-germinated aberrant appressorial swellings (squares) and undifferentiated germlings (triangles) following conidial germination on an HP surface for 24 h (n = 371 conidia examined over 3 biological replicates; biological replicates are colour coded; bars represent Mean ± SEM). **b**. Table to show the total number of DEGs, upregulated genes (p_{adj} <0.01; mod-lfc >1) and downregulated genes (p_{adj} <0.01; mod-lfc < -1) of Δ*pmk1 versus* Guy11, Δ*mst12 versus* Guy11 and Δ*hox7 versus* Guy11 at 14 h during appressorium development. **c**. Heatmap showing levels of relative transcript abundance between Δ*pmk1 versus* Guy11, Δ*mst12 versus* Guy11 and Δ*hox7 versus* Guy11 of a common set of 709 genes. For all heatmaps, the levels of expression are represented as moderated logarithmic fold change (mod_lfc) (blue= downregulated in mutants versus Guy11; red= upregulated in mutants versus Guy11. **d**. Heatmap showing levels of relative transcript abundance between Δ*pmk1 versus* Guy11 and Δ*hox7 versus* Guy11 of 1942 *M. oryzae* genes. **e**. Table to show the most representative cellular pathways found among 1942 genes with overlapping expression profiles in Δ*pmk1* and Δ*hox7*. **f**. Bar charts to show mean normalized counts of gene expression of cyclin, CDK-related, and DNA damage response (DDR) pathway-related genes during appressorium development in Guy11, Δ*pmk1*, Δ*mst12* and Δ*hox7* mutants. **g**. Heatmap to show relative transcript abundance of autophagy-related genes in Δ*pmk1*, Δ*mst12* and Δ*hox7* mutants compared to Guy11.
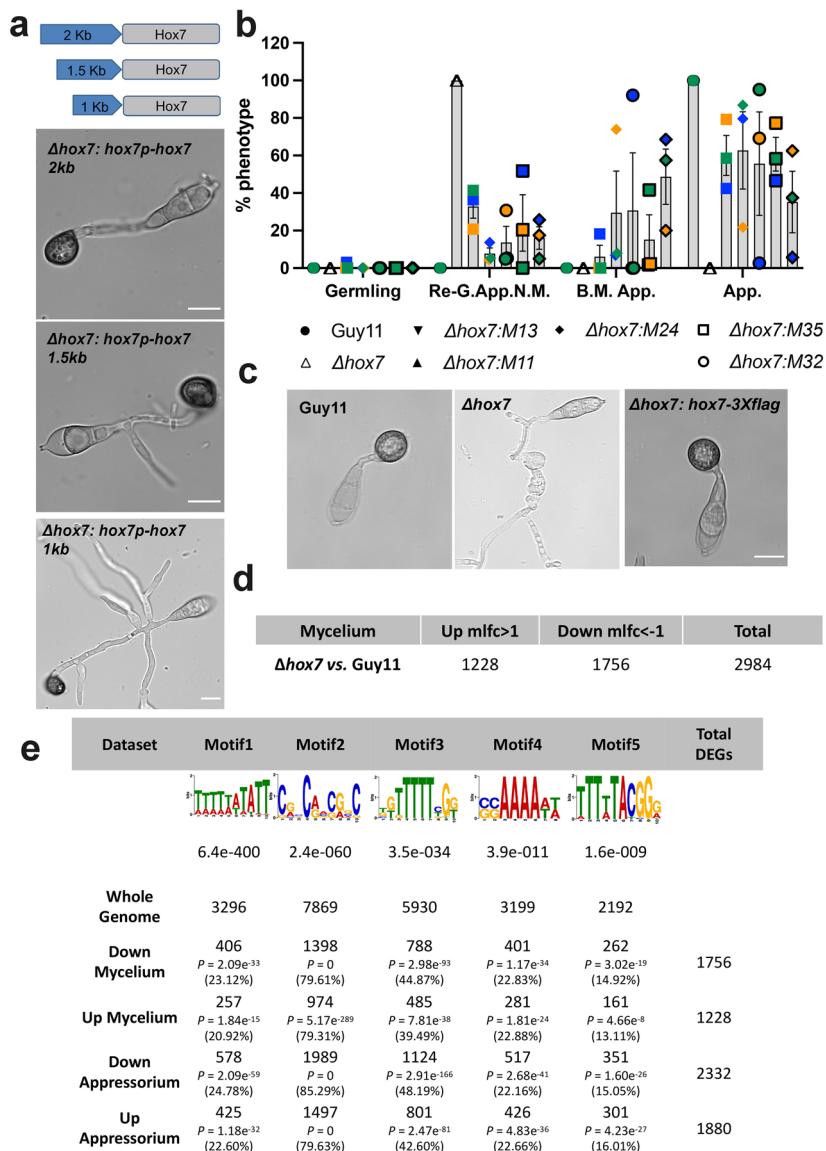
Extended Data Fig. 7 | Complementation of _Δhox7_ mutant and ChIP–seq analysis. a. Micrographs showing the extent of _Δhox7_ complementation upon re-introduction of _HOX7_ under control of three native promoter lengths (2 kb, 1.5 kb and 1kb), as shown in the schematic diagram. Conidia were inoculated on HP surface and incubated for 24 h (Bar = 10 μm). **b**. Bar chart to show the frequency of appressorium formation and range of aberrant infection structures formed by _Δhox7_ mutants expressing _HOX7_ under control of 1kb promoter (_Δhox7_:M11, _Δhox7_:M13), 1.5 kb promoter (_Δhox7_:M24) and 2 kb promoter fragment (_Δhox7_:M32, _Δhox7_:M35), n = 813 conidia examined in 3 biological replicates; each biological replicate is colour coded; the data are presented as Mean ± SEM) (legend X-axis- Re-G.App.N.M.: Re-germinated appressoria, non-melanised; B.M.App.: Branched melanised appressoria; App.: Appressoria). **c**. Micrographs to show appressorium development by Guy11, _Δhox7_ and _Δhox7:Hox7-3xFLAG_ (expressed under control of 2 kb native promoter fragment). Bar = 10 μm. **d**. Table to show the total number of DEGs, upregulated genes (p$_{adj}$ <0.01; mod-lfc >1) and downregulated genes (p$_{adj}$ <0.01; mod-lfc < -1) of _Δpmk1 versus_ Guy11, _Δmst12 versus_ Guy11 and _Δhox7 versus_ Guy11 during mycelium development determined by RNA-seq analysis. **e**. Table to show over-represented motifs in peaks determined in Hox7 ChIP–seq experiment by FIMO (https://meme-suite.org/meme/doc/fimo.html). Over-representation of each motif in specific sets of DEGs (up and downregulated in mycelium, or expressed during appressorium formation) was analysed using Fisher's exact test and _P_ values are indicated. The percentage value represents the proportion of the total pool of DEGs represented by that each set of motif-defined gene sets.
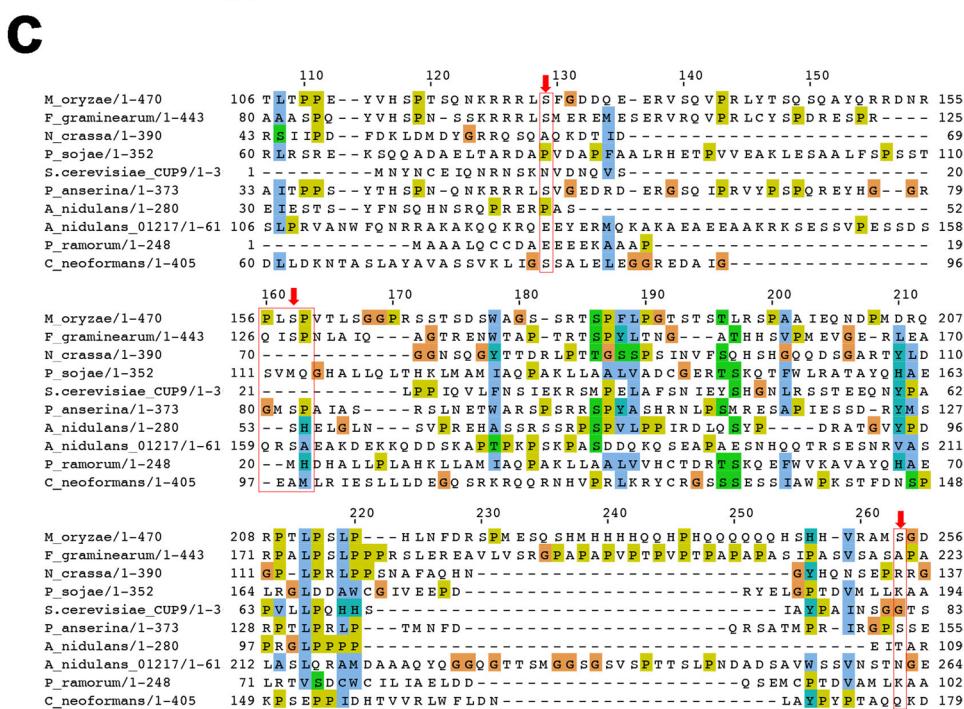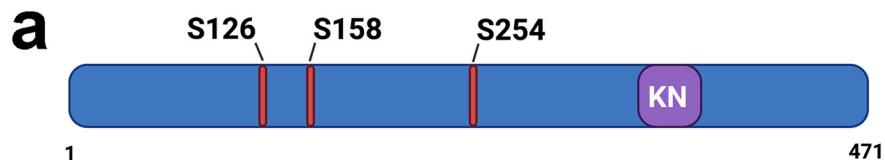
Extended Data Fig. 8 | See next page for caption.

Extended Data Fig. 8 | Hox7 conservation across fungi. a. Diagram to show phosphorylated serine residues identified by phosphoproteomic analysis in Hox7 corresponding to serine 126, 158 and 254. KN represents the PFAM domain homeobox KN (PF05920). **b**. Phylogenetic neighbour-joining tree to show conservation across fungal and oomycete species *Aspergillus nidulans, Phythopthora sojae, Phythopthora ramorum, Neurospora crassa, Cryptococcus neoformans, Saccharomyces cerevisiae, Fusarium graminearun, Magnaporthe oryzae* and *Podospora anserina*. **c**. Amino acid alignment of *HOX7* homologues identified using the Homeobox TFs InterPro term IPR001356 in the Fungal Transcription Factor Database http://ftfd.snu.ac.kr of *Aspergillus nidulans, Phythopthora sojae, Phythopthora ramorum, Neurospora crassa, Cryptococcus neoformans, Saccharomyces cerevisiae, Fusarium graminearun, Magnaporthe oryzae* and *Podospora anserina*.

a
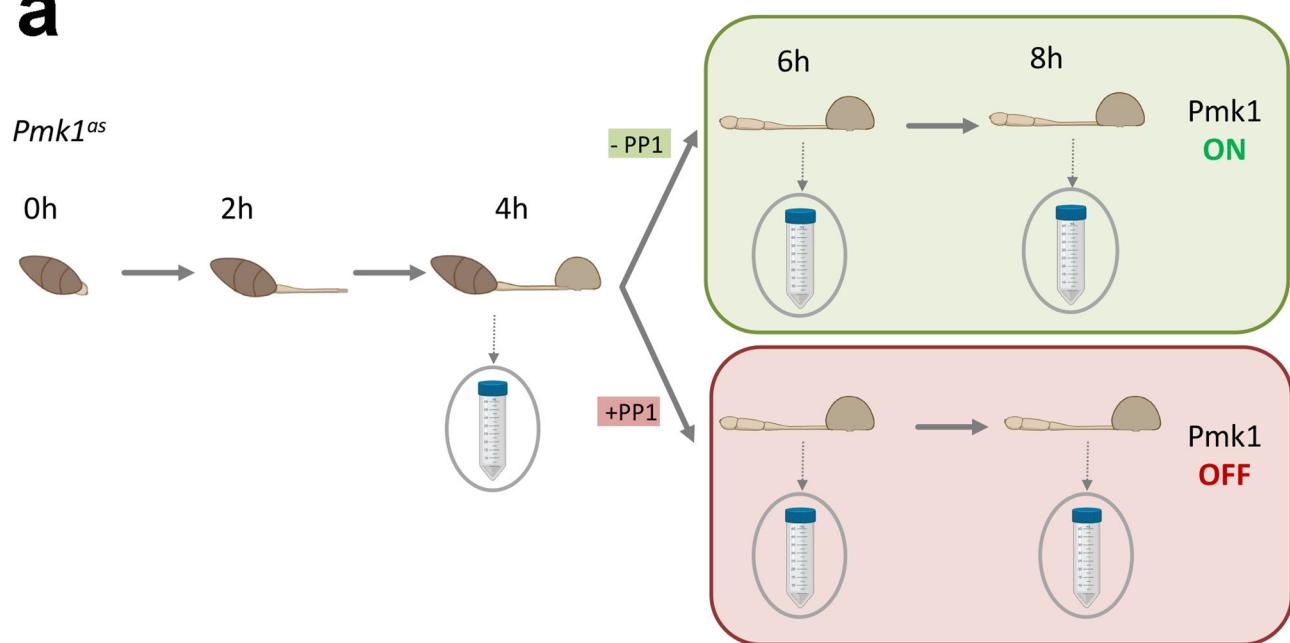
b

RLS[+80]FGDDQEER

c
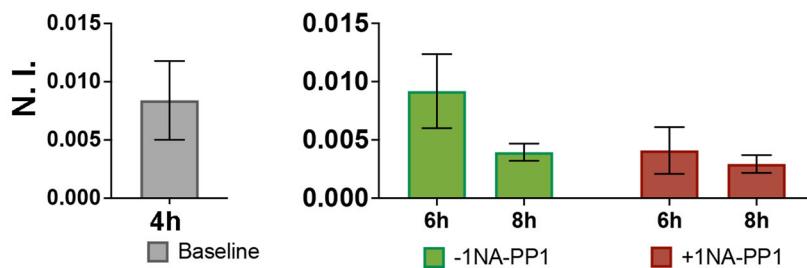
DNRPLS[+80]PVTLSGGPR

d
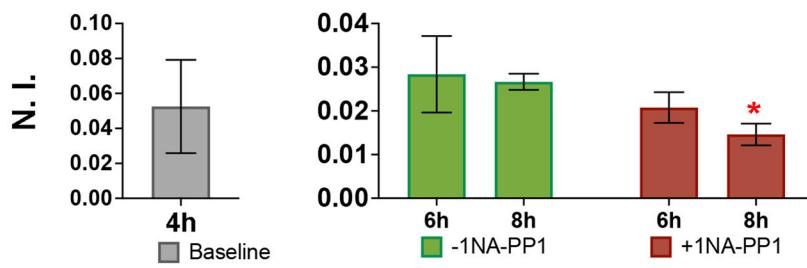
AM[+16]S[+80]GDEYM[+16]M[+16]EQHR
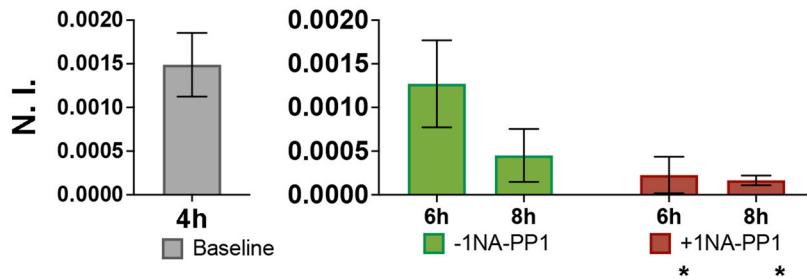
Extended Data Fig. 9 | See next page for caption.

Extended Data Fig. 9 | Phosphoproteomic analysis reveals Pmk1-dependent phosphorylation of Hox7 in *M. oryzae*. a. Diagram to show experimental design for PRM analysis to measure relative normalized intensities (R. N. I.) of peptides associated with serine 126, serine 158 and serine 254 residues of Hox7. The *pmk1ᵃˢ* conditional mutant was incubated on HP and germinated for 4 h (Baseline), 6 h and 8 h in the presence (+1NA-PP1 crimson bars) or absence (-1NA-PP1 green bars) of the ATP analogue Naphthyl-PP1. Falcon tubes represent sample collection. **b**. PRM showing R. N. I. of peptide associated with phosphorylated serine at 126 of Hox7 during appressorium development in *pmk1ᵃˢ* conditional mutant in the presence or absence of 1NA-PP1. Differences were assessed by a two-tailed unpaired t-test, using 2 biological replicates and 2 technical replicates per biological replicate, Mean ± SD. **c**. PRM showing R. N. I. of peptide associated with phosphorylated serine at 158 of Hox7 during appressorium development in *pmk1ᵃˢ* conditional mutant in the presence and absence of NA-PP1. Differences were assessed by a two-tailed unpaired t-test, 8 h ($P = 0.0316$), 2 biological replicates and 2 technical replicates per biological replicate, Mean ±SD. **d**. PRM showing R. N. I. of peptide associated with phosphorylated serine at 254 of Hox7 during appressorium development in *pmk1ᵃˢ* conditional mutant in the presence and absence of NA-PP1. Differences were assessed by a two-tailed unpaired t-test, 2 biological replicates and 2 technical replicates per biological replicate, Mean ±SD. Black asterisks below bar charts indicate that some peptides could not be detected in a biological or technical replicate. Red asterisks correspond to the significance of the *P* value.
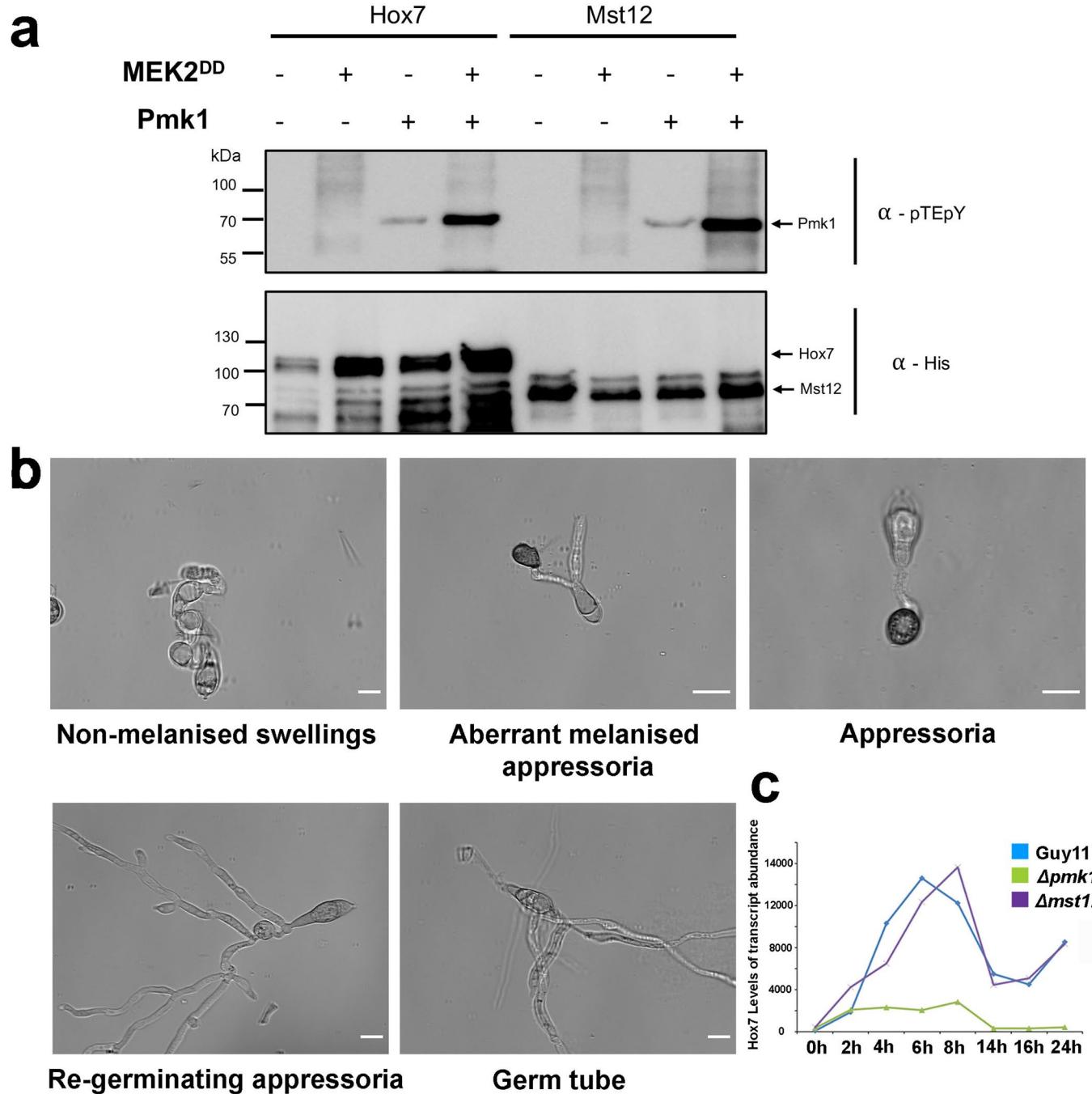
Extended Data Fig. 10 | Pmk1 activation by MEK2^DD, phenotypes of Δhox7 mutants expressing phosphomimetic alleles of Hox7 and temporal analysis of HOX7 gene expression. a. Western blot analysis of *in vitro* phosphorylation experiment of Pmk1 MAPK (GST- Pmk1)- with Hox7 (6xHis-SUMO-Hox7t-342) and Mst12 (6xHis-MBP-Mst12) in the presence or absence of the activated MEK^DD.. Proteins were immunoblotted with appropriate antisera (listed on the right). Arrows indicate expected band sizes. Phosphorylation of the Pmk1 MAPK was detected by α-pTEpY antibody in the presence of MEK^DD. His-tagged proteins were detected with α-His antibody. **b**. Micrographs to show representative phenotypes of germlings of Δhox7 mutants expressing phosphomimetic alleles of Hox7 incubated on HP surfaces for 24 h, as quantified in Fig. 7b (Bar= 10 μm). **c**. Line graph fo show temporal analysis of *HOX7* transcript abundance in wild type Guy11 (blue), and Δpmk1 (green) and Δmst12 (purple) mutants during a time course of appressorium development measured by RNA-seq analysis.

nature portfolio

Corresponding author(s): Nicholas. J. Talbot and Miriam Oses-Ruiz

Last updated by author(s): Aug 22, 2021

Reporting Summary

Nature Portfolio wishes to improve the reproducibility of the work that we publish. This form provides structure for consistency and transparency in reporting. For further information on Nature Portfolio policies, see our Editorial Policies and the Editorial Policy Checklist.

Statistics

For all statistical analyses, confirm that the following items are present in the figure legend, table legend, main text, or Methods section.

n/a	Confirmed	
☐	☒	The exact sample size (*n*) for each experimental group/condition, given as a discrete number and unit of measurement
☐	☒	A statement on whether measurements were taken from distinct samples or whether the same sample was measured repeatedly
☐	☒	The statistical test(s) used AND whether they are one- or two-sided *Only common tests should be described solely by name; describe more complex techniques in the Methods section.*
☒	☐	A description of all covariates tested
☒	☐	A description of any assumptions or corrections, such as tests of normality and adjustment for multiple comparisons
☐	☒	A full description of the statistical parameters including central tendency (e.g. means) or other basic estimates (e.g. regression coefficient) AND variation (e.g. standard deviation) or associated estimates of uncertainty (e.g. confidence intervals)
☐	☒	For null hypothesis testing, the test statistic (e.g. *F*, *t*, *r*) with confidence intervals, effect sizes, degrees of freedom and *P* value noted *Give P values as exact values whenever suitable.*
☒	☐	For Bayesian analysis, information on the choice of priors and Markov chain Monte Carlo settings
☒	☐	For hierarchical and complex designs, identification of the appropriate level for tests and full reporting of outcomes
☒	☐	Estimates of effect sizes (e.g. Cohen's *d*, Pearson's *r*), indicating how they were calculated

Our web collection on statistics for biologists contains articles on many of the points above.

Software and code

Policy information about availability of computer code

Data collection	Images were captured using a Photometrics Coolsnap HQ2 camera (Roper Scientific), under control of Metamorph v7.8 software (MDS Analytical Technologies). For mass spectrometry, MS/MS peak lists were exported using Discover v2.2 (Thermo Scientific).
Data analysis	Excel 16.52 for Mac 2021(Microsoft), Mascot 2.4.1 (Matrix Science), Scaffold v4.6.2 (Proteome Software), Tophat v 2.2.1 (John Hopkins Center for Computational Biology), DeSeq (https://bioconductor.org/packages/release/bioc/html/DESeq2.html), SignalP v. 4 (http://www.cbs.dtu.dk/services/SignalP/), GraphPad Software, Inc. Prism v8.1 (https://www.graphpad.com), Leica Application Suite X, version 3.1.5 (Leica, Wetzlar, Germany), MEME and MEME-ChIP (https://meme-suite.org/meme/index.html).

For manuscripts utilizing custom algorithms or software that are central to the research but not yet described in published literature, software must be made available to editors and reviewers. We strongly encourage code deposition in a community repository (e.g. GitHub). See the Nature Portfolio guidelines for submitting code & software for further information.

Data

Policy information about availability of data

All manuscripts must include a data availability statement. This statement should provide the following information, where applicable:

- Accession codes, unique identifiers, or web links for publicly available datasets
- A description of any restrictions on data availability
- For clinical datasets or third party data, please ensure that the statement adheres to our policy

All data that support the findings of this paper are available from the corresponding author on request. RNA-seq data described in this study has been submitted to European Nucleotide Archive ENA https://www.ebi.ac.uk/ena/submit. Appressorial RNA-seq data under accession number PRJEB36580 and mycelial RNA-seq data under accession number PRJEB44745. ChIP-seq data described in this study has been submitted to Gene Expression Omnibus under the accession number

GSE182534 (https://www.ncbi.nlm.nih.gov/geo/query/acc.cgi?acc=GSE182534). Proteomic data described in this study has been deposited into the ProteomeXchange Consortium via PRIDE (Perez-Riverol et al., 2019) partner repository with the dataset identifier: PXD025700 and 10.6019/PXD025700. The parallel reaction monitoring data has been made publicly available through PanoramaWeb (https://panoramaweb.org/84ne1U.url) and the corresponding ProteomeXchange ID for the data is: PXD028052 (http://proteomecentral.proteomexchange.org/cgi/GetDataset?ID=PXD028052). Scripts for the analysis and prediction of the peaks of ChIP-seq experiments have been publicly deposited in github (https://github.com/threadmaper/sequence-under-peaks). M. oryzae genome database used in this study was http://fungi.ensembl.org/Magnaporthe_oryzae/Info/Index. All Magnaporthe oryzae strains generated in this study are freely available upon request from the corresponding authors.

Field-specific reporting

Please select the one below that is the best fit for your research. If you are not sure, read the appropriate sections before making your selection.

☒ Life sciences   ☐ Behavioural & social sciences   ☐ Ecological, evolutionary & environmental sciences

For a reference copy of the document with all sections, see nature.com/documents/nr-reporting-summary-flat.pdf

Life sciences study design

All studies must disclose on these points even when the disclosure is negative.

Sample size	Sample sizes were as large as practicable for observations of appressorium function and virulence studies based on previous studies where estimates have provided statistically significant findings. Format power analysis was carried out when relevant. In all cases we used from two to six biological replicates for experiments, as that is standard practice for studies in our field to ensure reproducibility of the presented results (for example: Ryder et al., 2019 Nature 574, pages423–427; Ludwig et al., 2021,Nature Microbiology 6, 722–730; Masachis et al., 2016, Nature Microbiology 1, Article number: 16043).
Data exclusions	No data were excluded
Replication	All experiments were subject to at least three biological replications unless otherwise stated. Technical replications were also carried out as stated in the text. Results were consistent between replication unless otherwise stated. Several independent transformants were used where it was necessary to show biological variation in results and to demonstrate reproducibility of observations with as much rigour as possible (e.g. Figure 7).
Randomization	Microscopy observation and quantification were from samples selected randomly and quantified independently several times. All the experiments were analysed equally with no subsampling. Randomization in experimental procedures (such as quantification of nuclei number, for example) was not necessary as we measured a physical value. Randomization was not necessary because researchers were comparing samples under well-controlled conditions or treatments. No animal or human subjects were used in this study and randomization is not generally used in this field. For virulence assays, plants were assigned to strains randomly. In virulence assay experiments different researchers performed independent replicates of the same experiment to avoid any bias.
Blinding	Blind testing was not routinely carried out in the study as it was not relevant to most of the experiments carried out. Blinding was not necessary because every experiment was quantified at least two independent times with several technical replicates. Blind testing of virulence phenotypes was carried out as an independent check wherever possible.

Reporting for specific materials, systems and methods

We require information from authors about some types of materials, experimental systems and methods used in many studies. Here, indicate whether each material, system or method listed is relevant to your study. If you are not sure if a list item applies to your research, read the appropriate section before selecting a response.

Materials & experimental systems

n/a	Involved in the study
☐	☒ Antibodies
☒	☐ Eukaryotic cell lines
☒	☐ Palaeontology and archaeology
☒	☐ Animals and other organisms
☒	☐ Human research participants
☒	☐ Clinical data
☒	☐ Dual use research of concern

Methods

n/a	Involved in the study
☐	☒ ChIP-seq
☒	☐ Flow cytometry
☒	☐ MRI-based neuroimaging

Antibodies

Antibodies used	Phospho-p44/42 MAPK (Erk1/2) (Thr202/Tyr204) (D13.14.4E) XP® 1. Supplier name: Cell Signalling Technology 2. Catalog number: #4370S 3. Clone name: D13.14.4E

4. Reference: 01/2019

5. Lot number: 24

6. Validation: Primary antibody Phospho-p44/42 MAPK (Erk1/2) (Thr202/Tyr204) (D13.14.4E) XP® was used to detect phosphorylated Pmk1 on western blotting (Dilution 1:2000) as previous studies in Magnaporthe oryzae [1,2]. According to manufacturer's database, this antibody has been widely used to detect MAP Kinase (Erk1 and Erk2) when dually phosphorylated at Thr202 and Tyr204 of Erk1 (Thr185 and Tyr187 of Erk2).

Link to manufacturer's website: https://www.cellsignal.com/products/primary-antibodies/phospho-p44-42-mapk-erk1-2-thr202-tyr204-d13-14-4e-xp-rabbit-mab/4370

Anti-rabbit IgG, HRP-linked Antibody

1. Supplier name: Cell Signalling Technology

2. Catalog number: #7074S

3. Reference: 07/2018

4. Lot number: 28

5. Validation: This secondary antibody is conjugated to horseradish peroxidase (HRP) for chemiluminescent detection and was used to detect the primary antibody Phospho-p44/42 MAPK (Erk1/2) (Thr202/Tyr204) (D13.14.4E) XP® on western blotting (Dilution 1:5000).

Link to manufacturer's website: https://www.cellsignal.com/products/secondary-antibodies/anti-rabbit-igg-hrp-linked-antibody/7074

HRP Anti-6x His tag ® Antibody

1. Supplier name: Abcam

2. Catalog number: ab1187

3. Lot number: GR3248851-2

4. Validation: Primary antibody Anti-6x His tag ® is conjugated to horseradish peroxidase (HRP) for chemiluminescent detection and was used to detect Hox7 (6xHis-SUMO-Hox7t-342) and Mst12 (6xHis-MBP-Mst12 on western blotting (Dilution 1:5000). According to manufacturer's database, this antibody has been widely used to detect recombinant proteins 6xHis tagged.

Link to manufacturer's website: https://www.abcam.com/hrp-6x-his-tag-antibody-ab1187.html

References

1. Li X, Gao C, Li L, Liu M, Yin Z, Zhang H, et al. MoEnd3 regulates appressorium formation and virulence through mediating endocytosis in rice blast fungus Magnaporthe oryzae. Dean R, editor. PLOS Pathog. 2017;13: e1006449. doi:10.1371/journal.ppat.1006449

2. Yu R, Shen X, Liu M, Liu X, Yin Z, Li X, et al. The rice blast fungus MoRgs1 functioning in cAMP signaling and pathogenicity is regulated by casein kinase MoCk2 phosphorylation and modulated by membrane protein MoEmc2. PLOS Pathog. 2021;17: e1009657. doi:10.1371/JOURNAL.PPAT.1009657

Validation | Validation details are provided above for antibody used.

ChIP-seq

Data deposition

☒ Confirm that both raw and final processed data have been deposited in a public database such as GEO.

☒ Confirm that you have deposited or provided access to graph files (e.g. BED files) for the called peaks.

Data access links
May remain private before publication.

To review GEO accession number GSE182534
https://www.ncbi.nlm.nih.gov/geo/query/acc.cgi?acc=GSE182534

Files in database submission

GEO-ChIP-seq-Hox7-and-Mst12.xlsx
IC_rep1_hox7.fq.gz
IC_rep1_mst12.fq.gz
IC_rep2_hox7.fq.gz
IC_rep2_mst12.fq.gz
IC_rep3_hox7.fq.gz
IP_rep1_hox7.fq.gz
IP_rep1_mst12.fq.gz
IP_rep2_hox7.fq.gz
IP_rep2_mst12.fq.gz
IP_rep3_hox7.fq.gz
rep1_hox7.bed
rep1_mst12.bed
rep2_hox7.bed
rep2_mst12.bed
rep3_hox7.bed

| Genome browser session (e.g. UCSC) | ChIP-seq data were mapped to M. oryzae genome v.8 (MG8 https://www.ncbi.nlm.nih.gov/assembly/GCF_000002495.2) using BWA aligner v. 0.5.7. Peaks were identified by MACS2 version 2.1.1 66 with the following parameters: -g 41027733 -q 0.1 --bdg ---nomodel --extsize 180 --broad --broad-cutoff 0.1. Sequences under the peaks were predicted ± 2kb flanks and analysed using Python bespoke scripts (https://github.com/threadmaper/sequence-under-peaks). |

Methodology

Replicates	Data for the reported Hox7 ChIP-seq experiment are based on ChIP-seq peaks from three independent replicates. Data for the reported Mst12 ChIP-seq experiment are based on ChIP-seq peaks from two independent replicates.
Sequencing depth	ChIP-seq libraries were sequenced on Illumina HiSeq2500 in single read with 50nt read length in BGI Genomics (Hong Kong, China). Sequencing produced approximately 20 to 30 million reads per sample.
Antibodies	For hox7 ChIP-seq Anti-Flag® M2 Affinity Gel; M2, monoclonal; Anti-ddddk, Anti-dykddddk, Monoclonal ANTI-FLAG M2 antibody produced in mouse; Cat#:A2220-1ML; Sigma For Mst12 ChIP-seq GFP-Trap® Agarose Beads (Chromotek);monoclonal anti-Green Fluorescent Protein (GFP) single domain antibody (sdAb); Cat#gta-100; Chromotek
Peak calling parameters	ChIP peaks were identified with MACS2 version 2.1.1 with the following parameters: -g 41027733 -q 0.1 --bdg ---nomodel --extsize 180 --broad --broad-cutoff 0.1. Sequences under the peaks were predicted ± 2kb flanks and analysed using Python bespoke scripts (https://github.com/threadmaper/sequence-under-peaks)
Data quality	Threshold of False discovery rate (FDR) was set at at 0.1 and the peaks consistent across the replicates were further used in the annotation.
Software	Python 2.7.15 fastp 0.20.1 samtools-1.5 hisat2-2.1.0 pysam 0.11.2.2 bwa-0.5.7 macs2 version 2.1.1.20160309 pyranges-0.0.95 homer-4.6 bedtools-2.28.0 IGV_v2.4.6